

RESEARCH ARTICLE SUMMARY

IMMUNOGENOMICS

Single-cell RNA-seq reveals new types of human blood dendritic cells, monocytes, and progenitors

Alexandra-Chloé Villani,^{*†} Rahul Satija,^{*} Gary Reynolds, Siranush Sarkizova, Karthik Shekhar, James Fletcher, Morgane Griesbeck, Andrew Butler, Shiwei Zheng, Suzan Lazo, Laura Jardine, David Dixon, Emily Stephenson, Emil Nilsson, Ida Grundberg, David McDonald, Andrew Filby, Weibo Li, Philip L. De Jager, Orit Rozenblatt-Rosen, Andrew A. Lane, Muzlifah Haniffa,[†] Aviv Regev,[†] Nir Hacohen[†]

INTRODUCTION: Dendritic cells (DCs) and monocytes consist of multiple specialized subtypes that play a central role in pathogen sensing, phagocytosis, and antigen presentation. However, their identities and interrelationships are not fully understood, as these populations have historically been defined by a combination of morphology, physical properties, localization, functions, developmental origins, and expression of a restricted set of surface markers.

RATIONALE: To overcome this inherently biased strategy for cell identification, we performed single-cell RNA sequencing of ~2400 cells isolated from healthy blood donors and enriched for HLA-DR⁺ lineage⁻ cells. This single-cell profiling strategy and unbiased genomic classification, together with follow-up profiling and functional and phenotypic characterization of prospectively isolated subsets, led us to identify and validate six DC subtypes

and four monocyte subtypes, and thus revise the taxonomy of these cells.

RESULTS: Our study reveals:

1) A new DC subset, representing 2 to 3% of the DC populations across all 10 donors tested, characterized by the expression of *AXL*, *SIGLEC1*, and *SIGLEC6* antigens, named AS DCs. The AS DC population further divides into two populations captured in the traditionally defined plasmacytoid DC (pDC) and CD1C⁺ conventional DC (cDC) gates.

ON OUR WEBSITE
Read the full article at <http://dx.doi.org/10.1126/science.aaah4573>

This split is further reflected through AS DC gene expression signatures spanning a spectrum between cDC-like and pDC-like gene sets. Although AS DCs share properties with pDCs, they more potently activate T cells. This discovery led us to reclassify pDCs as the originally described “natural interferon-producing cells (IPCs)” with weaker T cell proliferation induction ability.

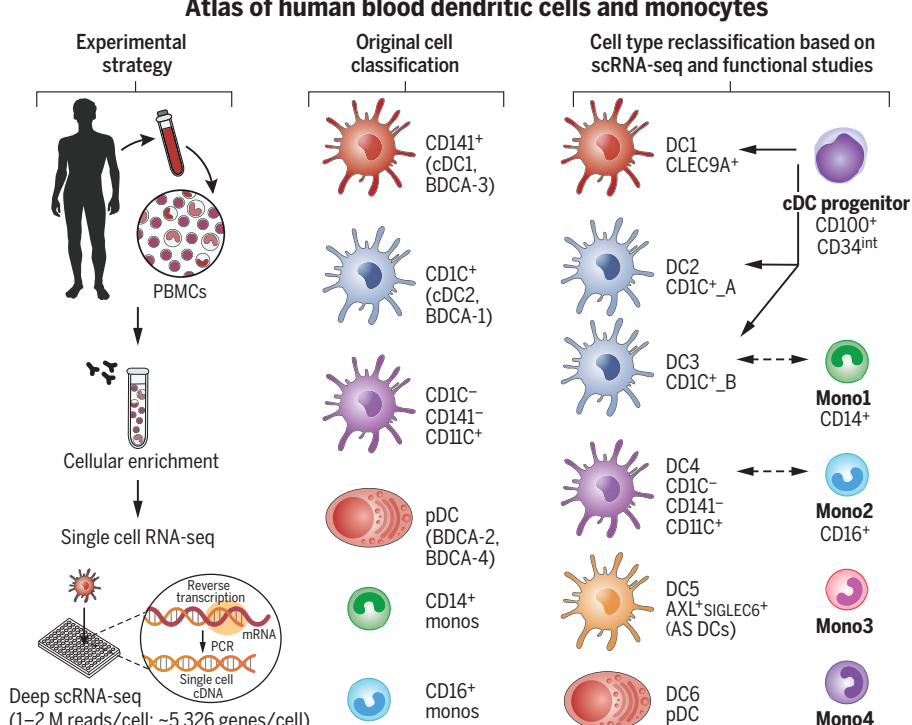
2) A new subdivision within the CD1C⁺ DC subset: one defined by a major histocompatibility complex class II-like gene set and one by a CD14⁺ monocyte-like prominent gene set. These CD1C⁺ DC subsets, which can be enriched by combining CD1C with CD32B, CD36, and CD163 antigens, can both potently induce T cell proliferation.

3) The existence of a circulating and dividing cDC progenitor giving rise to CD1C⁺ and CLEC9A⁺ DCs through in vitro differentiation assays. This blood precursor is defined by the expression of CD100⁺ CD34^{int} and observed at a frequency of ~0.02% of the LIN HLA-DR⁺ fraction.

4) Two additional monocyte populations: one expressing classical monocyte genes and cytotoxic genes, and the other with unknown functions.

5) Evidence for a relationship between blastic plasmacytoid DC neoplasia (BPDCN) cells and healthy DCs.

CONCLUSION: Our revised taxonomy will enable more accurate functional and developmental analyses as well as immune monitoring in health and disease. The discovery of AS DCs within the traditionally defined pDC population explains many of the cDC properties previously assigned to pDCs, highlighting the need to revisit the definition of pDCs. Furthermore, the discovery of blood cDC progenitors represents a new therapeutic target readily accessible in the bloodstream for manipulation, as well as a new source for better in vitro DC generation. Although the current results focus on DCs and monocytes, a similar strategy can be applied to build a comprehensive human immune cell atlas. ■



Establishing a human blood monocyte and dendritic cell atlas. We isolated ~2400 cells enriched from the healthy human blood lineage⁻ HLA-DR⁺ compartment and subjected them to single-cell RNA sequencing. This strategy, together with follow-up profiling and functional and phenotypic characterization, led us to update the original cell classification to include six DCs, four monocyte subtypes, and one conventional DC progenitor.

The list of author affiliations is available in the full article online.

*These authors contributed equally to this work.

†Corresponding author. Email: cvillani@broadinstitute.org (A.-C.V.); m.a.haniffa@newcastle.ac.uk (M.H.); aregev@broadinstitute.org (A.R.); nhacohen@mgh.harvard.edu (N.H.)
Cite this article as A.-C. Villani et al., Science 356, eaah4573 (2017). DOI: 10.1126/science.aaah4573

RESEARCH ARTICLE

IMMUNOGENOMICS

Single-cell RNA-seq reveals new types of human blood dendritic cells, monocytes, and progenitors

Alexandra-Chloé Villani,^{1,2*}† Rahul Satija,^{1,3,4*} Gary Reynolds,⁵ Siranush Sarkizova,¹ Karthik Shekhar,¹ James Fletcher,⁵ Morgane Griesbeck,⁶ Andrew Butler,^{3,4} Shiwei Zheng,^{3,4} Suzan Lazo,⁷ Laura Jardine,⁵ David Dixon,⁵ Emily Stephenson,⁵ Emil Nilsson,⁸ Ida Grundberg,⁸ David McDonald,⁵ Andrew Filby,⁵ Weibo Li,^{1,2} Philip L. De Jager,^{1,9} Orit Rozenblatt-Rosen,¹ Andrew A. Lane,^{1,7} Muzlifah Haniffa,^{5,10+} Aviv Regev,^{1,11,12†} Nir Hacohen^{1,2†}

Dendritic cells (DCs) and monocytes play a central role in pathogen sensing, phagocytosis, and antigen presentation and consist of multiple specialized subtypes. However, their identities and interrelationships are not fully understood. Using unbiased single-cell RNA sequencing (RNA-seq) of ~2400 cells, we identified six human DCs and four monocyte subtypes in human blood. Our study reveals a new DC subset that shares properties with plasmacytoid DCs (pDCs) but potently activates T cells, thus redefining pDCs; a new subdivision within the CD1C⁺ subset of DCs; the relationship between blastic plasmacytoid DC neoplasia cells and healthy DCs; and circulating progenitor of conventional DCs (cDCs). Our revised taxonomy will enable more accurate functional and developmental analyses as well as immune monitoring in health and disease.

Dendritic cells (DCs) are mononuclear phagocytes found in blood, lymphoid organs, and all tissues. One of their central functions is to ingest materials such as pathogens, present processed epitopes to T cells, and regulate innate and adaptive immune responses (1–3). DCs are heterogeneous and consist of multiple subtypes with unique functions that have been defined over the past decade in mice and humans. However, it is unclear how many DC subtypes exist, how they are related to each other, and how they differ from other mononuclear phagocytes.

Numerous studies have shown that human dendritic cells express high levels of major histocompatibility complex (MHC) class II (HLA-DR), a molecule essential for antigen presentation, and lack key markers of T cells, B cells, natural killer (NK) cells, granulocytes, and monocytes. In the blood, DC subtypes include CD1C⁺ conventional DCs (cDCs), consisting of either CD141⁺ or CD1C⁺ cells, and plasmacytoid DCs (pDCs), consisting of CD123⁺ cells. cDCs are effective at antigen-specific stimulation of CD4⁺ and CD8⁺ T cells, whereas pDCs specialize in producing type I interferons in response to viruses. pDCs and cDC subtypes differ in their expression of numerous sensors, pathways, and effectors, and play distinct roles in the immune response (1–3).

The different DC subtypes have historically been defined by a combination of morphology, physical properties, localization, molecular markers, functions, and developmental origins, converging to the current model described above (1–3). However, the definition of DCs is still likely to be biased by the limited markers available to identify, isolate, and manipulate the cells. Such biases, in turn, would alter the assignment of function and ontogeny to each DC subtype.

To overcome some of these limitations, we used single-cell RNA sequencing (scRNA-seq) (4, 5) to better assess the diversity of blood DCs and monocytes, leading us to identify new subtypes of DCs and monocytes, refine their existing classification, and pinpoint a precursor of cDCs in the blood. Using discriminative markers associated with the newly defined DC subtypes,

we also assessed the functions of some of the DC subtypes. Overall, our analysis provides a relatively unbiased and comprehensive map of human blood DCs and monocytes.

Strategy for discovery and validation of DC and monocyte subtypes

To determine the subtypes of DCs and monocytes in human blood, we developed an experimental and computational strategy to (i) perform single-cell RNA sequencing on DCs and monocytes derived from a single healthy individual; (ii) identify clusters of cells that are similar to each other; (iii) find discriminative markers per cluster; (iv) prospectively isolate cells corresponding to key clusters using newly identified surface markers; (v) validate the identity of the sorted cells using scRNA-seq; (vi) confirm the existence of these cell types in up to 10 independent healthy individuals; and (vii) perform functional analyses for selected cell types.

Single-cell profiling of blood DCs and monocytes

We analyzed blood DC and monocyte populations from Ficoll-enriched cells that were isolated by fluorescence-activated cell sorting (FACS) (Fig. 1A) excluding cells expressing markers of B, T, and NK cells (6). For DCs, we sampled LIN[−]HLA-DR⁺CD14[−] cells across the CD11C⁺ fraction (to enrich for CD141⁺ and CD1C⁺ cDCs) and the CD11C[−] fraction (to enrich for CD123⁺ pDCs) (Fig. 1B). For monocytes, we sampled LIN[−]CD14^{+/++} cells (including classical CD14⁺⁺CD16[−], intermediate CD14⁺⁺CD16⁺, and nonclassical CD14⁺CD16⁺⁺). We used additional markers (DCs: CD123, CD141, CD1C; monocytes: CD14, CD16) to create overlapping gates that comprehensively and evenly sample DCs and monocytes (6).

To define subpopulations and identify useful markers for further isolation, we performed deep scRNA-seq using a modified Smart-Seq2 protocol (6), followed by sequencing of ~1 million to 2 million paired-end reads per cell (7, 8). Of 768 DCs and 372 monocytes initially profiled in the selected individual for discovering subsets, we focused on 742 DCs and 339 monocytes that passed quality control (QC) filters (6) with an average of 5326 unique genes detected per cell. In subsequent validation and characterization phases, we additionally profiled ~1200 cells.

Unbiased classification of LIN[−]HLA-DR⁺CD14[−] subsets

We defined six cell clusters within the LIN[−]HLA-DR⁺CD14[−] population using unsupervised analysis that did not rely on known markers of DCs. Briefly, we identified 595 genes exhibiting high variability across single cells, reduced the dimensionality of these data with principal components analysis (PCA), and identified five significant PCs using a previously described permutation test (6, 9). We used these PC loadings as input to *t*-distributed stochastic neighbor embedding (*t*-SNE) (10) for visualization, and clustered cells using a graph-based approach similar to one

*These authors contributed equally to this work. †Corresponding author. Email: villani@broadinstitute.org (A.-C.V.); m.a.haniffa@newcastle.ac.uk (M.H.); aregev@broadinstitute.org (A.R.); nir.hacohen@mgh.harvard.edu (N.H.).

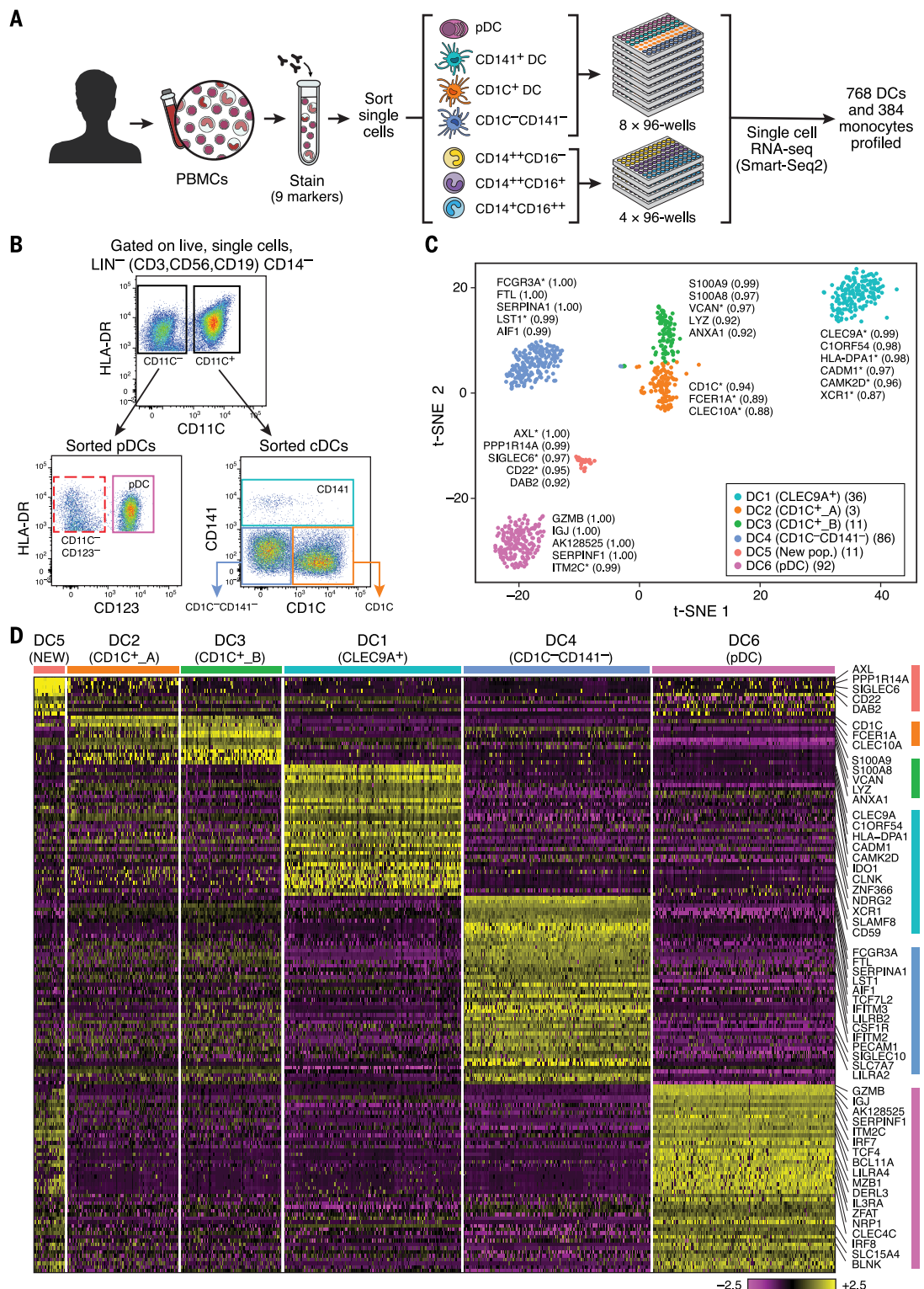
Fig. 1. Human blood DC heterogeneity delineated by single-cell RNA sequencing.

(A) Workflow of experimental strategy: (i) isolation of human PBMCs from blood; (ii) sorting single DCs (8×96 -well plates) and monocytes (4×96 -well plates) into single wells, using an antibody cocktail to enrich for cell fractions; (iii) single-cell transcriptome profiling.

(B) Gating strategy for single-cell sorting: DCs were defined as live, $\text{LIN}^-(\text{CD3}, \text{CD56}, \text{CD19}) \text{CD14}^-$ HLA-DR $^+$ cells. Three loose overlapping gates were drawn as an enrichment strategy to ensure a comprehensive and even sampling of all populations: $\text{CD11C}^+ \text{CD14}^+$ (CD141; turquoise), $\text{CD11C}^+ \text{CD1C}^+$ (CD1C; orange), $\text{CD11C}^+ \text{CD141}^- \text{CD1C}^-$ ("double negative"; blue), and $\text{CD11C}^- \text{CD123}^+$ plasmacytoid DCs (pDCs; purple); 24 single cells from these four gates were sorted per 96-well plate. A fifth gate ($\text{CD11C}^- \text{CD123}^-$; red dashed) was subsequently investigated (see Fig. 6). **(C)** t-SNE analysis of DCs ($n = 742$). Numbers of successfully profiled single cells per cluster: DC1 ($n = 166$); DC2 ($n = 105$); DC3 ($n = 95$); DC4 ($n = 175$); DC5 ($n = 30$); DC6 ($n = 171$). The number of discriminative genes with AUC cutoff ≥ 0.85 is reported in brackets next to each cluster ID. Up to five top discriminators are listed next to each cluster; number in brackets refers to AUC value. Colors indicate unbiased DC classification via graph-based clustering. Each dot represents an individual cell. **(D)** Heat map reports scaled expression [$\log \text{TPM}$ (transcripts per million) values] of discriminative gene sets for each cluster defined in Fig. 1C with AUC cutoff ≥ 0.85 . Color scheme is based on z-score distribution from -2.5 (purple) to 2.5 (yellow). Right margin color bars highlight gene sets specific to the respective DC subset.

recently developed for mass cytometry data (6, 11). We observed six clusters numbered DC1 to DC6 as follows: two clusters mapping closely to the well-established DC subsets, with cluster DC1 mapping to CD141 $^+$ DCs and cluster DC6 to pDCs (based on the post hoc overlap of transcript and surface marker expression); two clusters

containing the CD1C $^+$ cDCs, cluster DC2 (CD1C_A) and cluster DC3 (CD1C_B); a cluster corresponding to the poorly characterized CD141 $^-$ CD1C $^-$ population, cluster DC4; and one cluster that does not correspond to any of the known blood DC subtypes, cluster DC5 (Fig. 1C and fig. S1).



We identified 242 genes [area under curve (AUC) ≥ 0.85] that best classified cells into these six putative cell populations (Fig. 1D and fig. S2A; see tables S1 and S2 for a list of markers, including surface markers). Although cluster DC1 mapped most closely to CD141 $^+$ DCs, this commonly used CD141 (*THBD/BDC-A-3*) marker

was a poor discriminator for this cluster, being also expressed by cells captured in clusters DC5 and DC6 (pDCs) (fig. S2B). Because *CLEC9A* appeared to be a perfect discriminative surface marker for the DC1 cluster, we refer to this

subset henceforth as CLEC9A⁺ DCs. Clusters DC2 and DC3 mapped to CD1C⁺ DCs. CD1C was the best and sole marker uniquely shared by both clusters. The DC4 cluster mapped to the CD14⁺ CD1C⁻ population and was accurately delineated

by *FCGR3A*/CD16. The DC5 cluster was best defined by the surface markers *AXL* and *SIGLEC6*. Finally, the DC6 cluster mapped to pDCs. However, several markers commonly used to identify pDCs (e.g., *IL3RA*/CD123, *CLEC4C*/CD303)

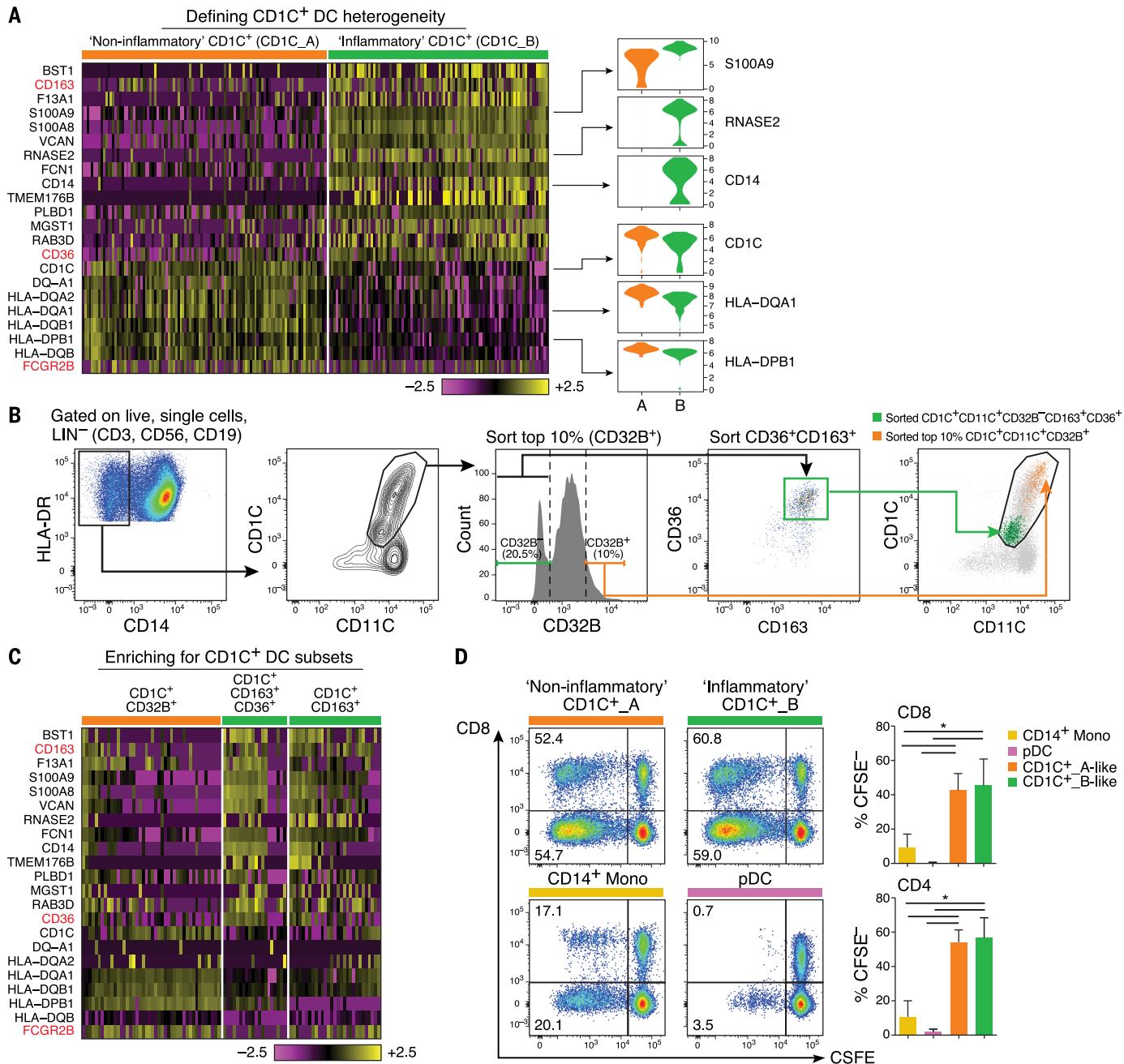


Fig. 2. Definition and validation of CD1C⁺ DC subsets. (A) Heat map showing scaled expression (log TPM values) of discriminative gene sets defining each CD1C⁺ DC subset with AUC cutoff ≥ 0.75 . Color scheme is based on z-score distribution, from -2.5 (purple) to +2.5 (yellow). Violin plots illustrate expression distribution of candidate genes across subsets on the x axis (orange for CD1C_A/DC2; green for CD1C_B/DC3). In red are three markers used for subsequent enrichment strategy: CD163, CD36, and FCGR2B/CD32B (AUC = 0.63). (B) Enrichment gating strategy of CD1C⁺ DC subsets [LIN(CD3, CD19, CD56)⁻HLA-DR⁺CD14⁻CD1C⁺CD11C⁺]. The CD1C_A/DC2 subset was further enriched by sorting on the 10% brightest CD32B⁺ cells (orange gate); the CD1C_B/DC3 subset was enriched by sorting on CD32B⁺CD163⁺CD36⁺

cells (green gate) or on CD32B⁺CD163⁺. Right: Overlay of the two sorted CD1C⁺ DC populations; 47 single cells were sorted from the green and orange gates in a 96-well plate for profiling. (C) Heat map reporting scaled expression (log TPM values) of scRNA-seq data from three cell subsets defined by CD1C⁺CD32B⁺, CD1C⁺CD36⁺CD163⁺, and CD1C⁺CD163⁺. Either CD1C⁺CD36⁺CD163⁺ or CD1C⁺CD163⁺ population recapitulated the CD1C_B/DC3 signature. (D) Proliferation of allogeneic CD4⁺ and CD8⁺ T cells 5 days after coculture with CD14⁺ monocytes, pDCs, CD1C_A/DC2 DCs (CD1C⁺CD32B⁺), and CD1C_B DC3 (CD1C⁺CD163⁺). Left: Representative pseudocolor dot plot. Right: Bar graphs of composite data ($n = 3$, mean \pm SEM, * $P < 0.05$, paired t test).

were also expressed in the population defined by the DC5 cluster, leading us to define a new combination of markers that distinguish pDCs from the DC5 population. Altogether, we identified sets of discriminative markers that can be used in combination to isolate cell populations corresponding

to known DC subsets (but with higher purity) as well as to previously uncharacterized subsets.

Two subpopulations within CD1C⁺ DCs

The CD1C⁺ DCs were distributed across two clusters with similar numbers of cells, which

we termed CD1C_A (cluster DC2) and CD1C_B (cluster DC3). Comparing the two clusters, the CD1C_B cells were distinguished by their expression of a strong unique signature that includes acute and chronic inflammatory genes (12–14) such as *CD14*, *S100A9*, and *S100A8*, whereas CD1C_A cells

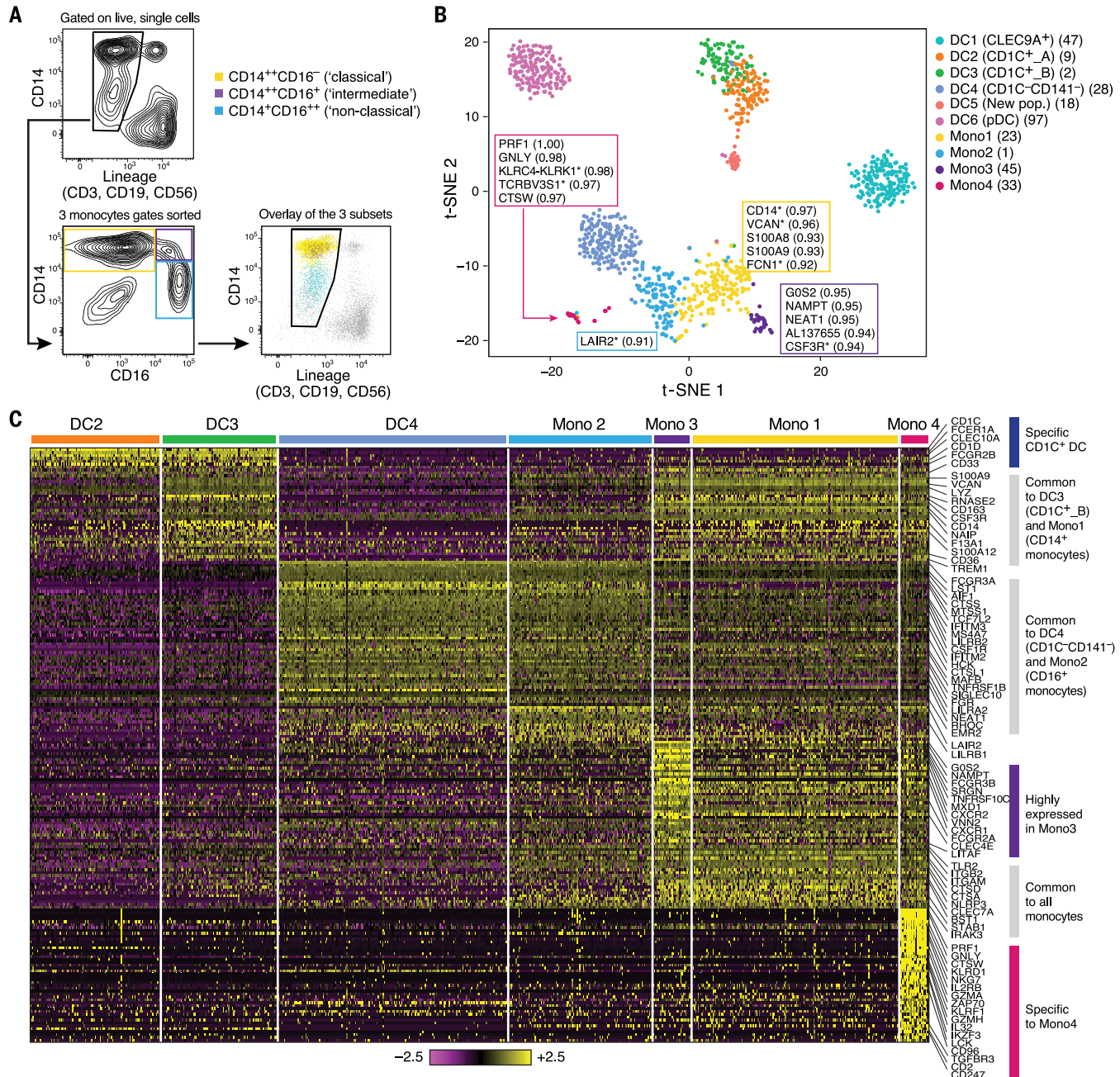


Fig. 3. Human blood monocyte heterogeneity. (A) Gating strategy for monocyte single-cell sorting. Monocytes were enriched by first gating on LIN(CD3, CD19, CD56)⁻CD14⁺⁺, followed by three loose overlapping gates defined by relative expression of CD14 and CD16 for comprehensive sampling of CD14⁺⁺CD16⁻ (yellow), CD14⁺⁺CD16⁺ (purple), and CD14⁺CD16⁺⁺ (blue); 32 cells from each gate were sorted per 96-well plate profiled. Bottom right: Dot plot shows overlay of the sorted populations. (B) t-SNE analysis incorporating monocytes ($n = 337$ successfully profiled) and DCs ($n = 742$). Number of successfully profiled single monocytes per transcriptionally defined clusters includes Mono1 ($n = 148$), Mono2 ($n = 137$), Mono3 ($n = 31$), and Mono4 ($n =$

21). The number of discriminative genes with $AUC \geq 0.85$ (combined analysis of DC and monocyte data sets) is reported in brackets next to cluster ID. Up to five top discriminators are listed next to each cluster; the number in brackets next to each gene refers to AUC value. Colors indicate unbiased DC and monocyte clustering from graph-based clustering. Each dot represents an individual cell. (C) Heat map reporting scaled expression (log TPM values) of discriminative gene sets for each monocyte subsets with $AUC \geq 0.85$ (see fig. S3B for detailed heat map). Color scheme is based on z-score distribution, from -2.5 (purple) to 2.5 (yellow). Color bars in right margin highlight gene sets of interest.

were marked only by slightly higher levels of MHC class II genes (Fig. 2A and table S3).

We validated the presence of the two populations by prospective isolation based on newly identified markers, followed by scRNA-seq. To isolate these cells by flow sorting, we developed a panel incorporating surface markers derived from the set of uniquely expressed genes: *FCGR2B*/*CD32B* for CD1C_A, and *CD163* and *CD36* for CD1C_B subsets (Fig. 2B). scRNA-seq of prospectively isolated cells from each subset recapitulated the original split observed in CD1C+ DCs (Fig. 2C). Unlike monocytes and pDCs, both CD1C_A and CD1C_B subsets (isolated with the newly identified markers) were potent stimulators of naïve T cell proliferation ($P < 0.05$, paired *t* test), consistent with the known functional characteristics of cDCs (Fig. 2D). Activation of both CD1C subsets with lipopolysaccharide (LPS), R848 (a TLR7/TLR8 agonist), and polyinosine-polycytidine [poly(I:C)] highlighted functional differences between these subsets (fig. S3 and table S4), with CD1C_A secreting higher levels of the immune mediators CCL19, interleukin-10 (IL-10), IL-12B, and IL-18. Thus, scRNA-seq revealed unappreciated heterogeneity in this particular subset, leading to new hypotheses about the functions of CD1C+ DCs.

Discovering monocyte subsets and their relationships to DC subsets

Some key genes known to be associated with monocytes were also expressed by CD1C_B (cluster DC3) and CD141+CD1C- (cluster DC4) cells (e.g., *CD14* and *FCGR3A/CD16*, respectively). To analyze the relationships between monocytes and DCs, we profiled 372 single blood monocytes (Fig. 1A and Fig. 3A). On the basis of 339 monocytes that passed QC, we identified four clusters (Fig. 3B and fig. S4A) distinguished by 102 classifier genes ($AUC \geq 0.85$; Fig. 3C, fig. S4B, and table S5). The two largest clusters, Mono1 and Mono2, contained the CD14++CD16- ("classical") and CD14+CD16++ ("nonclassical") monocytes, respectively. However, Mono1 and Mono2 also included 88 of the 124 cells derived from the "intermediate" monocyte gate (CD14++CD16+) (fig. S4A), demonstrating that the intermediate monocytes do not form a homogeneous population. The two smaller clusters, Mono3 and Mono4, contained 40 of the 124 intermediate cells and expressed many of the Mono1 (classical monocyte) signature genes. Mono3 expresses a unique combination of genes that have the potential to affect cell cycle, differentiation, and trafficking (e.g., *MDI*, *CXCR1*, *CXCR2*, *VNN2*) whereas Mono4 distinctively expressed a cytotoxic gene signature (e.g., *PRF1*, *GNLV*, *CTSW*) resembling previously reported "natural killer dendritic cells," in addition to coexpressing Mono1 gene set (15–17) (Fig. 3C and fig. S4B). We conclude that the previously defined classical and nonclassical subtypes are contained in two distinct clusters (Mono1 and Mono2, respectively), but that the intermediate monocytes are far more heterogeneous than previously appreciated, being distributed across two known and two new clusters (fig. S4A).

All monocyte subtypes shared a signature that distinguishes them collectively from CD1C+ DC (cluster DC2 and DC3), CLEC9A+ DC (cluster DC1), and pDC (cluster DC6) populations (e.g., *ITGAM/CD11B*, *ITGB2/CD18*, *TLR2*, and *CLEC7A*) (Fig. 3, B and C, and fig. S4B). Thus, despite coexpressing genes such as *CD14* and *S100A8*, Mono1 and CD1C_B/DC3 cells were part of distinct clusters (Fig. 3, B and C). CD1C+ DCs (DC2 and DC3) expressed unique markers (e.g., *CDIC*, *CLEC10A*, *FCER1A*, *FCGR2B*, and *CD1D*) enriched for antigen processing ($P < 2.66 \times 10^{-10}$), MHC II ($P < 1.79 \times 10^{-8}$), and leukocyte activation ($P < 1.14 \times 10^{-6}$) gene ontology (GO) terms (Fig. 3C and table S6) (6). In contrast, Mono1 cells were enriched for defense response ($P < 2.15 \times 10^{-14}$), inflammatory response ($P < 9.59 \times 10^{-14}$), and chemotaxis ($P < 6.77 \times 10^{-10}$) genes.

Finally, we interrogated the relationship between CD16-expressing CD141-CD1C- cells (cluster DC4) and CD16+ monocytes (cluster Mono2). Although the two populations shared many genes (e.g., *FCGR3A*), they formed distinct clusters (Fig. 3B) defined by a unique discriminative gene set (Fig. 3C and tables S7 and S8). DC4 cells were enriched for type I interferon signaling pathway ($P < 1.53 \times 10^{-13}$) and response to virus ($P < 4.77 \times 10^{-9}$) GO terms, whereas Mono2 cells were enriched for immune system process ($P < 1.09 \times 10^{-14}$) and leukocyte migration ($P < 3.57 \times 10^{-8}$) GO terms. Although we conclude that monocytes and DCs are distinct from each other in the steady state, our data do not address potential interconversion between cell fates or distinct ontogeny.

AXL⁺SIGLEC6⁺ population and its relation to cDCs and pDCs

As described above, a population emerged from the unbiased cluster analysis (cluster DC5; Fig. 1), defined by coexpression of unique markers (e.g., *AXL*, *SIGLECI*, *SIGLEC6*, and *CD22/SIGLEC2*) (Fig. 4A, fig. S5A, and tables S1 and S2). Flow cytometry analysis of peripheral blood mononuclear cells (PBMCs) from 10 independent donors confirmed the existence of AXL⁺SIGLEC6⁺ cells ("AS DCs") within the original DC gate (Fig. 4B) at a frequency of 2 to 3%, consistent with what was originally observed in the initial scRNA-seq analysis (30 of 768 DCs; Fig. 1C). scRNA-seq profiling of prospectively sorted AS DCs (isolated with the gating strategy in Fig. 4B) showed that the newly sorted cells clustered together with the original cluster (Fig. 4C and fig. S5B), validating our enrichment strategy.

AS DCs exhibited a spectrum of states based on gene expression (Fig. 4D) defined by cells enriched for a pDC-like signature (e.g., *IL3RA*, *IGJ*, *NRPI*, *MZB1*) and cells enriched for a cDC-like signature (*IFI30*, *ITGAX*, *LY86*, *GLIPR2*, *FGR*, *LYZ*, *ENTPDI*). We validated this observation by flow cytometry, using the surface markers *IL3RA/CD123* and *ITGAX/CD11C* that respectively correlated with pDC and cDC gene signatures (Fig. 4, B and D). We exploited the combinatorial expression of AXL, SIGLEC6, CD123, and CD11C (at both mRNA and protein levels) to prospectively isolate the ends of this spectrum

representing two putative AS DC subtypes (see gating strategy in Fig. 4B), and further validated their identities by scRNA-seq (Fig. 4E and fig. S5, C to F). Across all 10 individuals tested, the two AS DC subpopulations represented a very small fraction of the Lin- HLA-DR+ populations (Fig. 4F). Notably, lower levels of AXL and SIGLEC6 protein were associated with increased HLA-DR, CD11C, and CD11C, whereas higher levels of AXL and SIGLEC6 were associated with increased CD123, CD303, and CD141 and decreased HLA-DR (fig. S5, C to J). This latter relationship was also observed by t-SNE analysis of flow cytometry data, where a peninsula with graded expression of AS DCs was located at the base of the CD1C+ DC cluster and adjacent to the pDC cluster (Fig. 4G). Trajectory mapping of these cells across different levels of the surface markers CD123 and CD11C further indicated that AS DCs form a continuum from a pDC transcriptional state to a CD1C+ DC transcriptional state (fig. S5, C to F). Taken together, our data suggest that AXL⁺SIGLEC6⁺ DCs are related but not identical to cDCs or pDCs.

pDCs are phenotypically and functionally distinct from CD123⁺CD11C⁻ AS DCs

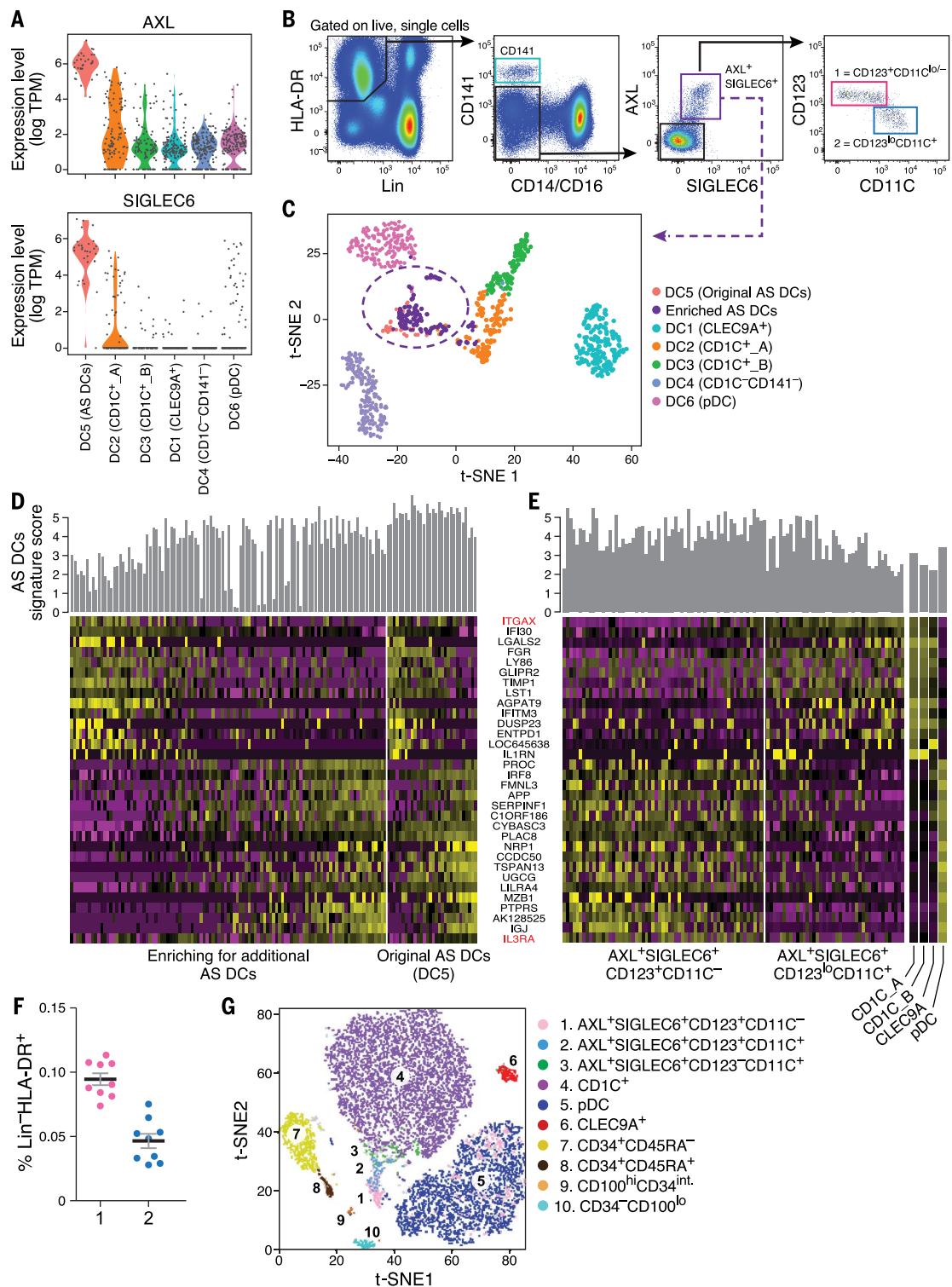
Because pDCs and AXL⁺SIGLEC6⁺CD123⁺CD11C⁻ DCs shared expression of many genes (Fig. 4, D and E, and fig. S6A), we assessed whether these cell types also shared functional properties. We found that the genes specifically expressed by pDCs, but not by AS DCs, were associated with the known biological properties of pDCs. This includes, for example, genes associated with pathogen sensing and induction of type I interferons (*IRF7*, *TLR7*, *SLC15A4*, and *PACSIN1*), secretion (e.g., *DERL3*, *LAMP5*, and *SCAMP5*), and the pDC master regulator transcription factor *TCF4*, along with its binding targets (e.g., *SLA2*, *PTCRA*, *PTPRCAP*) (Fig. 5A and fig. S6A) (18, 19). In contrast, CD123⁺CD11C⁻ AS DCs expressed cDC markers, including *CD2*, *CX3CRI*, *CD33/SIGLEC3*, *CD5*, and *SIGLECI/CD169*, both at protein and mRNA levels (Fig. 5A and fig. S6, A to C). pDCs were also morphologically distinct from AS DCs. Both AS DC subsets possessed the same cerebriform nucleus and cytoplasmic features of cDCs (Fig. 5B). We hypothesized that although CD123⁺CD11C⁻ AS DCs expressed pDC markers, including *IL3RA/CD123* and *CLEC4C/CD303* (fig. S5, G to J), they are functionally distinct from pDCs.

To compare the functional properties of "pure" pDCs to AS DCs and cDCs, we used the markers identified in our study to isolate pure pDCs by excluding AS DCs, CLEC9A+ DCs, CD1C+ DCs, and monocytes by FACS. As expected, pure pDCs produced their hallmark cytokine, interferon- α (IFN- α), while AS DCs produced negligible amounts of IFN- α upon Toll-like receptor 9 (TLR9) stimulation ($P < 0.001$; Fig. 5C). In contrast, the CD123^{hi}CD11C⁺ AS DC subset secreted IL-12p70 at similar levels to other cDCs, while pure pDCs and CD123^{hi}CD11C⁻ AS DCs did not produce IL-12p70 ($P < 0.01$; Fig. 5C). Other factors, such as IL-8, were produced at high levels by the CD123⁺CD11C⁻ AS DC subset but not by pDCs

Fig. 4. Identification of AXL⁺SIGLEC6⁺ DCs (AS DCs). (A) Violin plots showing expression distribution of surface markers AXL and SIGLEC6. Other populations are depicted on the x axis; each dot represents an individual cell. (B) Flow cytometry gating strategy to identify AXL⁺SIGLEC6⁺ cells within human blood LIN(CD3, CD19, CD20, CD161)⁻ and HLA-DR⁺ mononuclear fraction. AXL⁺SIGLEC6⁺ cells were further distinguished by the relative expression of *IL3RA*/CD123 and *ITGAX*/CD11C [1 = CD123⁺CD11c^{-/lo} (pink); 2 = CD123^{lo}CD11c⁺ (blue)]. Data shown are a representative analysis of 10 healthy individuals.

(C) t-SNE analysis of all DCs ($n = 742$), along with prospectively profiled AXL⁺SIGLEC6⁺ single cells ($n = 105$), using gating strategy in (B) (sorted from purple gate). Newly isolated AS DCs overlap with the originally identified DC5 cluster ($n = 30$), indicated by purple dashed circle.

(D) Heat map reporting scaled expression (log TPM values) of discriminative gene sets (AUC cutoff ≥ 0.75), highlighting the expression continuum of AS DCs. Top bar graph defines the AS DCs population purity score based on the top 10 most discriminative genes (i.e., AXL, *PPPIR14A*, *SIGLEC6*, *CD22*, *DAB2*, *S100A10*, *FAM105A*, *MED12L*, *ALDH2*, and *LTK*). (E) Heat map reporting scaled expression (log TPM values) of prospectively enriched AS DCs populations ($n = 90$) isolated by relative *ITGAX*/CD11C and *IL3RA*/CD123 expression levels [red in (D)]; 43 single AXL⁺SIGLEC6⁺CD11C⁻ [pink gate in (B)] and 47 single AXL⁺SIGLEC6⁺CD11C⁺ gate in (B)] were sequenced. The average expression values of the original CD1C⁺ (combined DC2 and DC3), CD141⁺/CLEC9A⁺ (DC1), and pDC (DC6) single cells were used as reference to highlight enrichment of cDC-like and pDC-like gene sets. Top bar graph represents AS DC purity score. (F) Frequency (% mean \pm SEM) of AXL⁺SIGLEC6⁺CD123⁺CD11C^{-/lo} [population 1 (pink): 0.1 ± 0.014] and AXL⁺SIGLEC6⁺CD123^{lo}CD11C⁺ [population 2 (blue): 0.04 ± 0.01] as a percentage of LIN(CD3, CD19, CD20, CD161)⁻HLA-DR⁺ PBMCs. Scatterplot includes data from nine healthy individuals. (G) t-SNE analysis of flow cytometry data for LIN(CD3, CD19, CD20, CD161)⁻HLA-DR⁺CD14⁺CD16⁻ PBMCs based on the protein expression levels of AXL, SIGLEC6, CD1C, CD11C, CD22, CD33, CD34, CD45RA, CD100, CD123, CD303, and HLA-DR (see Fig. 6 for CD100^{hi}CD34^{int} population). Overlay of populations defined by conventional flow cytometry gating on clusters derived by t-SNE analysis is shown in the legend.



($P < 0.001$; fig. S6D). Finally, pure pDCs induced undetectable or low levels of T cell proliferation in response to LPS or LPS + R848 stimulation, respectively ($P < 0.05$; Fig. 5D). We conclude that “pure” IFN- α -producing pDCs (depleted of AS DCs) do not up-regulate CD86 (fig. S6, C and E), are diminished in their ability to induce T cell proliferation, and that contamination of AS DCs within the traditionally defined pDC gate is likely responsible for T cell stimulation activities measured in prior reports (18–20).

AS DCs stimulate T cell proliferation and are present in tonsils

Because AS DCs expressed the costimulator CD86 and components of antigen presentation, we hypothesized that they could stimulate T cell proliferation (fig. S6, A, C, and E). Strikingly, both AS DC subtypes were potent stimulators of allogeneic CD4 $^{+}$ and CD8 $^{+}$ T cell proliferation, unlike pDCs ($P < 0.01$), and were marginally superior to CD1C $^{+}$ and CLEC9A $^{+}$ DCs (Fig. 5E).

Similar to other DCs, AS DCs expressed CLA and CD62L but not CCR7 protein (fig. S6F), suggesting potential homing to peripheral tissue such as skin and lymph node from the circulation. Because CD123 $^{+}$ pDCs were observed in the T cell area of the human tonsil (21), we evaluated whether CD123 $^{+}$ AS DCs were also present by staining human tonsils with antibodies to CD123 and AXL. We found AS DCs adjacent to CD3 $^{+}$ T cells, admixed with CD123 $^{+}$ AXL $^{-}$ pDCs (Fig. 5F). Flow cytometry confirmed this finding, showing that the CD123 $^{+}$ CD11C $^{-}$ AS DCs represented 0.7% and CD123 $^{+}$ CD11C $^{+}$ AS DCs represented 1.7% of the CD45 $^{+}$ LIN $^{-}$ HLA-DR $^{+}$ fraction (Fig. 5F). Thus, AS DCs are able to stimulate T cells and are present in the T cell zones of tonsils.

Identification of circulating CD100 $^{\text{hi}}$ CD34 $^{\text{int}}$ cDC progenitors

Finally, we interrogated CD11C $^{+}$ CD123 $^{-}$ cells within the HLA-DR $^{+}$ CD14 $^{-}$ gate used for isolating DCs that were not considered in the initial analysis because they were not previously thought to include DCs (red dashed gate in Fig. 1B and updated gate in Fig. 6A used for these experiments). Analysis of CD11C $^{+}$ CD123 $^{-}$ scRNA-seq data revealed six clusters in this gate (fig. S7, A and B). Cells in cluster 6 expressed genes associated with hematopoiesis, DC progenitors, and genes essential for DC development (e.g., SATB1, RUNX2, KIT, HLX, ID2) (22–25) and were marked by high expression of the cell surface protein SEMA4D (CD100). We therefore hypothesized that cluster 6 could represent a progenitor population.

To assess the progenitor potential of this compartment, we cultured FACS-purified CD11C $^{+}$ CD123 $^{-}$ cells with MS5 stromal cells and cytokines that induce DC differentiation (6), based on a published human DC progenitor differentiation assay (26). After several days in culture, the cells were evaluated by flow cytometry, using a panel of antibodies that identify pDCs and CD1C $^{+}$ and CLEC9A $^{+}$ DCs (6), and by scRNA-Seq profiling of CD45 $^{+}$ immune cells for a more comprehensive assessment. For comparison, under the same con-

ditions, we monitored the differentiation potential of isolated pDCs, CD1C $^{+}$ and CLEC9A $^{+}$ DCs, and AS DC subtypes (see fig. S7, C and D).

After 7 days of culture, cells isolated from the CD11C $^{+}$ CD123 $^{-}$ gate gave rise to CLEC9A $^{+}$ and CD1C $^{+}$ DCs but not pDCs, according to flow cytometry and scRNA-seq analyses (Fig. 6B). We narrowed down the search for the progenitor cells to the CD45RA $^{+}$ CD39 $^{-}$ CD100 $^{+}$ pool of cells based on the unique cluster-6 marker CD100/SEMA4D (fig. S7B), along with candidate markers that we tested [based on DC progenitors in the bone marrow (CD45RA) and tissue DC (CD39) markers] (Fig. 6C, fig. S5J, fig. S6, B and F, and fig. S7, B to H). After iteratively testing each sorted population for differentiation potential, we discovered that only the CD100 $^{\text{hi}}$ CD34 $^{\text{int}}$ cells generated CLEC9A $^{+}$ and CD1C $^{+}$ DCs (Fig. 6C and fig. S7F). scRNA-seq of CD100 $^{\text{hi}}$ CD34 $^{\text{int}}$ cells mapped these cells to the original cluster 6, including the expression of the same DC differentiation and progenitor function genes (fig. S7B).

We validated the existence of CD100 $^{\text{hi}}$ CD34 $^{\text{int}}$ progenitors in 10 individuals, with a frequency of ~0.02% of the LIN $^{-}$ HLA-DR $^{+}$ fraction of PBMCs (Fig. 6D). These cells were morphologically primitive, possessing high nuclear-to-cytoplasmic ratios and circular or indented nuclei (Fig. 6D), in contrast to AS DCs, pDCs, and CD1C $^{+}$ and CLEC9A $^{+}$ DCs (Fig. 5B). Although CD100 $^{\text{hi}}$ CD34 $^{\text{int}}$ cells expressed HLA-DR and low levels of the costimulatory molecule CD86 (fig. S6E) and lymph node homing gene CCR7 (fig. S7, B and H), they had low T cell stimulatory potential (Fig. 5C), which suggests that these cells are not functional cDCs. Furthermore, CD100 $^{\text{hi}}$ CD34 $^{\text{int}}$ cells retained significant proliferative capacity ($P < 0.05$; Fig. 6E), in accordance with their primitive morphology, phenotype, and expression profile. Although CD100 $^{\text{hi}}$ CD34 $^{\text{int}}$ cells were CD117 $^{+}$ KIT $^{+}$ CD45RA $^{+}$ and CSFIR/CD115 $^{-}$, CD1C $^{-}$, CD141 $^{-}$, CD123 $^{-}$ —a profile similar to that of a previously reported circulating human DC progenitor (24, 27, 28)—they differ from the published progenitor in having a more primitive morphology and lacking CSF2R/CD116 and FLT3/CD135 expression (fig. S7, G and H).

Differentiation potential of AS DCs

When we seeded cultures with pDCs and CD1C $^{+}$ and CLEC9A $^{+}$ DCs, we found that they generally retained the same phenotype throughout the differentiation assay (Fig. 6F and fig. S7, I and J). Upon observing a gene expression spectrum of AS DC states that includes pDC-like and CD1C $^{+}$ -like DC signatures (fig. S5, C to F), we also seeded AS DCs to assess their potential to transition toward other DC subsets [ensuring no contamination with CD1C $^{+}$ and CLEC9A $^{+}$ DCs (fig. S7, I and J)]. After 7 days in culture, we observed cells with high levels of CD1C (frequency 40 to 50%, $n = 6$ donors) and rare cells with surface CLEC9A and CADM1 (0.5 to 0.8%) expression (Fig. 6F), irrespective of the FLT3L concentration used (Fig. 6F) or whether the culture was seeded with either of the two AS DC subpopulations representing both ends of the spectrum (fig. S7K). Notably, both AS DCs at day 0 and the cells differentiated from

AS DCs did not express BATF3 (a transcription factor required for terminal differentiation of CLEC9A $^{+}$ DCs), CADM1, or XCR1, which are key CLEC9A $^{+}$ DC discriminative markers (table S2) (23, 29–33) (fig. S5, D and E).

We found that AS DCs did not divide during the transition into CD1C $^{+}$ DCs, in contrast to CD100 $^{\text{hi}}$ CD34 $^{\text{int}}$ cells that divided and differentiated into CD1C $^{+}$ as well as CLEC9A $^{+}$ DCs. Furthermore, CD100 $^{\text{hi}}$ CD34 $^{\text{int}}$ differentiation into CD1C $^{+}$ DCs is not likely to transition through AS DCs, because CD100 $^{\text{hi}}$ CD34 $^{\text{int}}$ did not express AXL or SIGLEC6 genes at day 0 or during differentiation. AS DCs are thus functional cDCs that exist in a continuum of states in vivo (fig. S5, C to F), with the potential to transition toward CD1C $^{+}$ DCs.

Mapping malignant cells from patients to the healthy DC atlas

We leveraged our human DC atlas to compare pathogenic cells driving blastic plasmacytoid dendritic cell neoplasm (BPDCN), a rare and aggressive hematological malignancy previously known as NK cell leukemia/lymphoma (34, 35), to healthy DC populations. Because the ontogeny of these cells remains unclear (34–38), we performed scRNA-seq on CD45 $^{+}$ HLA-DR $^{+}$ CD123 $^{+}$ blasts from four BPDCN patients ($n = 174$ cells) (6). The first principal component highlighted gene sets clustering all four patients together with healthy blood pDCs (Fig. 6G). Analysis of BPDCN samples together with healthy DCs showed the highest overlap with pDC and AS DC gene expression signatures (fig. S8A). Because pure pDC and AS DC subsets coexpress many genes yet have distinct biological functions (Figs. 4 and 5), we further analyzed the genes overlapping among BPDCN, pure pDCs, and cDCs (fig. S8B). Despite sharing some pDC genes (e.g., NRPI, IL3RA, DERL3, LAMP5, PTCRA, and PTPRCAP), several key genes essential for pDC function were missing or were expressed only slightly in patient cells (e.g., CZMB, IRF7, CLEC4C/CD303, IRF4, and SLC15A4; fig. S8B). Only a small number of cDC genes were expressed in patient cells, including SIGLEC6, LTK, FCER1A, CD59, CADM1, and TMEM144. Note that all four patient samples shared a set of discriminative genes (fig. S8B and table S9) that included several genes expressed in B cells (e.g., FCRL4, IGLL1, TCL1A, and IGLL5; fig. S8C) or with hematopoietic progenitors (e.g., SOX4 and CLEC11A). Collectively, our analysis suggests that although BPDCN malignant cells express some key B cell markers, they are most closely related to pDCs.

Discussion

DCs and monocytes are defined according to a combination of molecular markers, functional properties, and ontogeny (39). However, it remains unclear whether the expression of existing markers tracks with the more complex internal states of cells. To address this question, we determined the states of blood DCs/monocytes through comprehensive profiling of gene expression at single-cell resolution, empirically inferred cell subtypes, identified optimal surface markers for purifying the hypothesized cell subtypes, and showed that prospectively

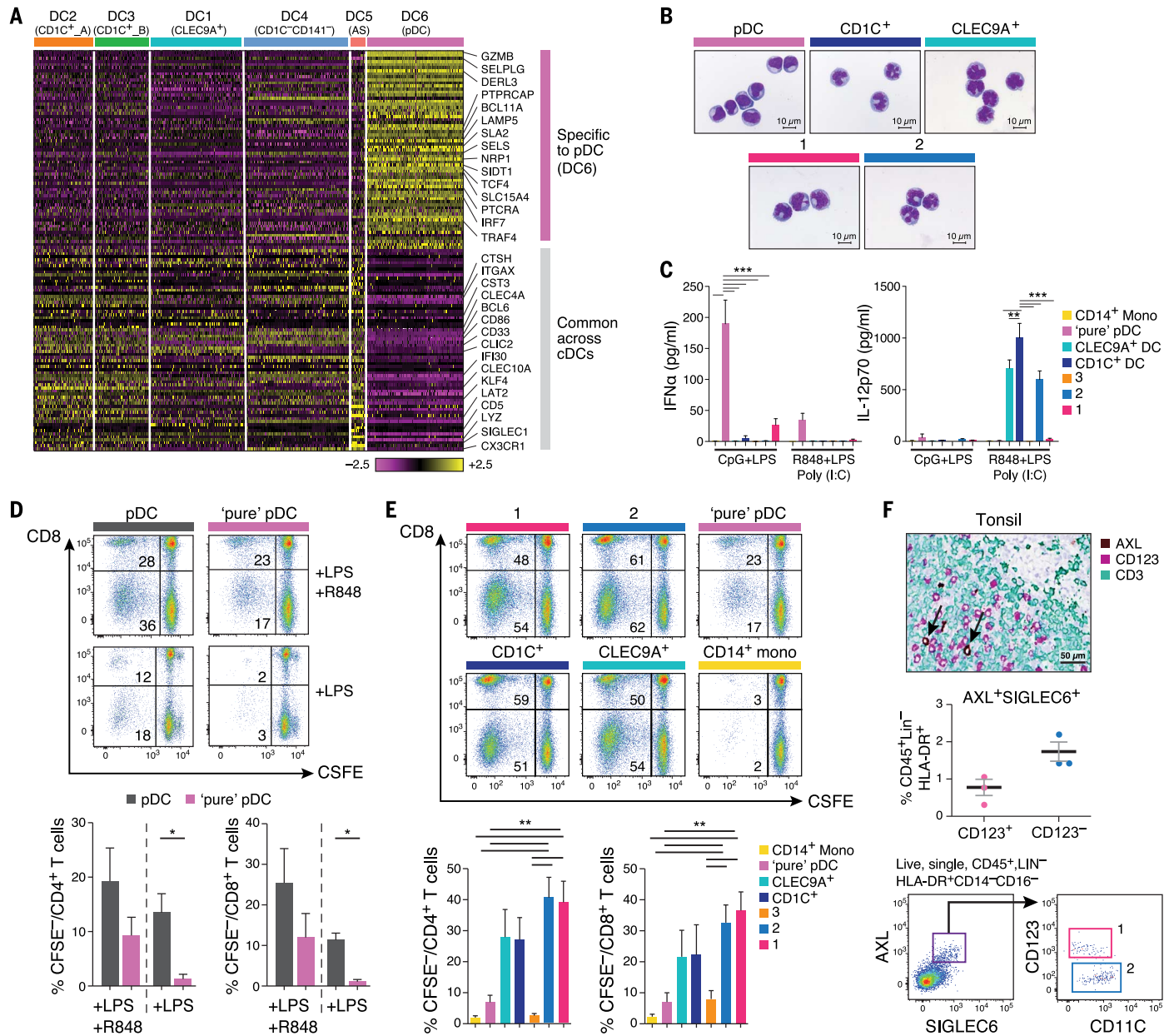


Fig. 5. Phenotypic and functional characterization of AS DCs and “pure” pDCs. (A) Heat map reporting scaled expression (log TPM values) of gene sets common between AS DCs (DC5) and cDCs (clusters DC1 to DC4), and genes uniquely expressed in pDCs (DC6). Gene sets were generated through K-means clustering using the doKmeans function in the Seurat package. (B) Morphology of pDCs, CD1C⁺ DCs, CLEC9A⁺ DCs, AXL⁺SIGLEC6⁺CD123^{lo}CD11C^{-lo}, and AXL⁺SIGLEC6⁺CD123^{lo}CD11C⁺ by Giemsa-Wright stain. Scale bar, 10 μ m. (C) IFN- α (left panel) and IL-12p70 (right panel) concentration in culture supernatant 24 hours after CpG and LPS stimulation ($n = 8$) or after LPS, R848, and poly(I:C) stimulation ($n = 4$) of CD14⁺CD16⁻ monocytes, pDCs, CLEC9A⁺ DCs, CD1C⁺ DCs, AXL⁺SIGLEC6⁺CD123^{lo}CD11C^{-lo} cells (1, pink), AXL⁺SIGLEC6⁺CD123^{lo}CD11C⁺ cells (2, blue), and CD100^{hi}CD34^{int} cells (3, beige). Composite data from four to eight donors is shown (mean \pm SEM; ** $P < 0.01$, *** $P < 0.001$, Mann-Whitney U test). (D) Proliferation of allogeneic CD4⁺ and CD8⁺ T cells 5 days after coculture with pDCs contaminated with AXL⁺SIGLEC6⁺ cells compared with pDCs devoid of AXL⁺SIGLEC6⁺ cells, in the context of LPS or LPS + R848 stimulation. Top: Representative pseudocolor dot plot. Bottom: Bar graphs of composite data ($n = 4$, mean \pm SEM, * $P < 0.05$, paired t test). (E) Proliferation of allogeneic CD4⁺ and CD8⁺ T cells 5 days after coculture with CD14⁺CD16⁻ monocytes, pDCs, CLEC9A⁺ DCs, CD1C⁺ DCs, AXL⁺SIGLEC6⁺CD123^{lo}CD11C^{-lo} (1, pink), AXL⁺SIGLEC6⁺CD123^{lo}CD11C⁺ (2, blue) cells, and CD100^{hi}CD34^{int} (3, beige) cells. Top: Representative pseudocolor dot plot. Bottom: Bar graphs of composite data ($n = 7$, mean \pm SEM, ** $P < 0.01$, paired t test). (F) Top: Immunohistochemical staining of human tonsil with AXL (brown), CD123 (purple), and CD3 (green). Brown arrows depict AXL⁺CD123⁺ cells adjacent to CD3⁺ T cells. Data shown are representative of four donors. Scale bar, 50 μ m. Middle: Frequency of AXL⁺SIGLEC6⁺CD123⁺ and CD123^{lo/-} cells in human tonsil determined by flow cytometry analysis, as a percentage of CD45⁺LIN(CD3, CD19, CD20, CD56, CD161)⁻HLA-DR⁺ cells (mean \pm SEM of three donors shown; AXL⁺SIGLEC6⁺CD123⁺, 0.7 \pm 0.2%; AXL⁺SIGLEC6⁺CD123^{lo/-}, 1.7 \pm 0.2%). Bottom: Representative pseudocolor dot plot of AXL⁺SIGLEC6⁺CD123⁺ (pop. 1, pink) and AXL⁺SIGLEC6⁺CD123^{lo/-} (pop. 2, blue) cells in human tonsil by flow cytometry analysis ($n = 3$).

color dot plot. Bottom: Bar graphs of composite data ($n = 4$, mean \pm SEM, * $P < 0.05$, paired t test). (E) Proliferation of allogeneic CD4⁺ and CD8⁺ T cells 5 days after coculture with CD14⁺CD16⁻ monocytes, pDCs, CLEC9A⁺ DCs, CD1C⁺ DCs, AXL⁺SIGLEC6⁺CD123^{lo}CD11C^{-lo} (1, pink), AXL⁺SIGLEC6⁺CD123^{lo}CD11C⁺ (2, blue) cells, and CD100^{hi}CD34^{int} (3, beige) cells. Top: Representative pseudocolor dot plot. Bottom: Bar graphs of composite data ($n = 7$, mean \pm SEM, ** $P < 0.01$, paired t test). (F) Top: Immunohistochemical staining of human tonsil with AXL (brown), CD123 (purple), and CD3 (green). Brown arrows depict AXL⁺CD123⁺ cells adjacent to CD3⁺ T cells. Data shown are representative of four donors. Scale bar, 50 μ m. Middle: Frequency of AXL⁺SIGLEC6⁺CD123⁺ and CD123^{lo/-} cells in human tonsil determined by flow cytometry analysis, as a percentage of CD45⁺LIN(CD3, CD19, CD20, CD56, CD161)⁻HLA-DR⁺ cells (mean \pm SEM of three donors shown; AXL⁺SIGLEC6⁺CD123⁺, 0.7 \pm 0.2%; AXL⁺SIGLEC6⁺CD123^{lo/-}, 1.7 \pm 0.2%). Bottom: Representative pseudocolor dot plot of AXL⁺SIGLEC6⁺CD123⁺ (pop. 1, pink) and AXL⁺SIGLEC6⁺CD123^{lo/-} (pop. 2, blue) cells in human tonsil by flow cytometry analysis ($n = 3$).

purified cell types corresponded to inferred subtypes based on scRNA-seq. Our study has generated a more accurate taxonomy that includes six DC subtypes and four monocyte subtypes, as well as a circulating, dividing progenitor of cDCs.

Previous studies classified human blood DCs into one pDC and two cDC populations. Our study identifies six DC populations: DC1 corresponds to the cross-presenting CD141⁺/BDCA-3⁺ cDC1, which is best marked by CLEC9A; DC2 and DC3 correspond to new subdivisions of the CD1C/BDCA-1⁺ cDC2; DC4 corresponds to CD1C⁺CD141⁻CD11C⁺ DC, which is best marked by CD16 and shares signatures with monocytes; DC5 is a unique DC subtype, AS DCs; and DC6 corresponds to the interferon-producing pDC, purer than previously identified pDC populations defined by standard markers (CD123, CD303/BDCA-2) and contaminated with AS DCs. In the process of addressing how DCs resemble monocytes, we also identified four monocyte subtypes: the two known ones, as well as two new ones that have not been functionally characterized. Although DC2/3 and DC4 shared an expression signature with monocytes, our data do not suggest how they acquired these shared modules (common precursor, interconversion, or independent convergence). Finally, we derived specific expression signatures for each DC and monocyte subtype, including transcription factors, cytokines, and cytokine receptors (fig. S9, A to F, and table S10), providing a resource for further understanding of subtype functions and ontogeny.

The CD1C/BDCA-1⁺ DC subdivision (DC2 and DC3) is further supported by parallel observations in their murine CD11b⁺ DC homologs (40–43), which comprise an Esam^{lo} subset with higher expression of myeloid genes such as *CD14* and potent cytokine production, and an Esam^{hi} subset with better MHC class II-dependent priming of CD4⁺ T cells (40, 41).

AS DCs, which were found within the pDC gate, formed a continuum between pDCs and CD1C⁺ DCs (fig. S5, C to F). Consistent with this observation, AS DCs were able to transition toward the CD1C⁺ DC state in vitro (with <1% of differentiated AS DCs phenotypically resembling CLEC9A⁺ DCs, which could be contaminants). However, because AS DCs (at both ends of the continuum) morphologically resemble cDCs and are able to stimulate T cell proliferation, yet do not proliferate themselves, they seem less likely to serve as a progenitor that generates cDCs and are more likely to be a functional DC variant that can be modulated to resemble CD1C⁺ DCs. Although AS DCs most closely resemble CD1C⁺ cDCs in basic functional properties and expression signatures, they are likely to have distinct functions because they localize to the T cell zone of tonsils and express several lectins, which recognize diverse glycans, and AXL, which interacts with apoptotic cells and Zika virus (44–46).

An unresolved question concerns the importance of AS DCs sharing an expression signature with pDCs. Consistent with our findings that AS DCs are found in the traditional pDC flow cytometry gate, a recently described human CD2^{hi} pDC subset (20) appears to correspond to AS DCs

based on expression of *CD2*, *AXL*, *CX3CRI*, *LYZ*, and *CD86* (fig. S6C), localization to tonsils, and a similar ability to trigger naïve T cell proliferation. Furthermore, a murine study identified noncanonical CX3CRI⁺CD8a⁺ cDCs (nc-cDCs), which express pDC and cDC signatures (e.g., CX3CRI, CD11c, and MHCII), do not produce IFN- α , and activate T cell proliferation (47, 48). Interestingly, pDCs and nc-cDCs require E2-2/TCF4 to develop, and reduced levels of E2-2 lead to higher ID2 and expression of cDC genes (18, 47, 48). Consistent with this finding, we observed E2-2/TCF4 expression in human pDCs (Fig. 5A), with decreasing levels of E2-2/TCF4 and increasing levels of ID2 as AS DCs transition to CD1C⁺ DCs (fig. S5, C to F). These findings suggest that AS DCs are similar to human CD2^{hi} pDCs and murine nc-cDCs.

The discovery of AS DCs led us to update the strategy for isolating pDCs. When we removed AS DCs from pDCs isolated with standard markers (e.g., CD123 and CD303), the resulting pDCs were highly attenuated in their ability to induce T cell proliferation and produce T cell stimulatory ligands (e.g., IL-12), consistent with reports that found several markers splitting pDCs into those that stimulate or do not stimulate T cells (18, 20, 49–52). We thus propose that our purer pDC population corresponds more closely to the “natural interferon-producing cells (IPCs)” (21, 53). These cells also appear to share more properties with plasma B cells than DCs, as indicated by morphology, higher expression of endoplasmic reticulum secretory machinery, known rearrangement at the Ig (immunoglobulin) locus, and expression of B cell-related transcripts. We also found that BPDCN cells share the pDC signature as well as additional B cell genes (e.g., *IGLL1*, *IGLL5*, and *TCL1A*). We conclude that even though pure pDCs fall into the MHC II-expressing gate, they have markers, gene signatures, and functions distinct from those of cDCs.

In contrast to AS DCs, the CD100^{hi}CD34^{int} cells appear to be cDC progenitors, judging by their primitive morphology, absence of cDC functions and signatures, and potent ability to proliferate and generate a large and equal number of CD1C⁺ DCs and CLEC9A⁺ DCs within 7 days of culture. The recently identified human pre-cDC (24–28), which has proliferative capacity and differentiates into CD1C⁺ and CD141⁺ DCs, appears to have some functional and phenotypical similarities to our CD100^{hi}CD34^{int} progenitors, even though our cells appear to be morphologically more primitive and lack the expression of CD116 and CD135, which were previously reported as markers (24). Single-cell profiling studies are needed to determine whether and how these precursors are related.

CD100^{hi}CD34^{int} cells also appear to be different from peripheral blood CD34^{hi} HSCs. Culturing of CD100^{hi}CD34^{int} cells gives rise only to CLEC9A⁺ DCs and CD1C⁺ DCs (and no other cell types) in 7 days. In contrast, peripheral blood CD34^{hi} HSCs under the same culture conditions for up to 14 days did not give rise to CLEC9A⁺ cDCs. Furthermore, CD100^{hi}CD34^{int} cells have a transcriptional signature distinct from that of blood CD34^{hi} HSCs. Mapping CD100^{hi}CD34^{int} to

other bone marrow progenitors may help to resolve the origin of these cells.

Our results have several implications. The discovery of several DC subsets will enable a more complete understanding of DCs in tissues, inflammation, and disease. Furthermore, the identification of circulating CD100^{hi}CD34^{int} progenitors provides a well-defined cell type for generating DCs in vitro and for therapeutic targeting. Our new strategy for isolating pure pDCs, combined with the knowledge that the functions of contaminating AS DCs were incorrectly attributed to pDCs, should lead to more definitive annotation of pDC functions with implications for their therapeutic application (54–56). More generally, our use of the DC atlas to understand BPDCN cells illustrates how single-cell analysis can pinpoint relationships of diseased cells to healthy cells. Finally, some susceptibility genes identified in human genetics association studies are expressed in the DCs and monocyte subsets defined in this study, suggesting new potential roles in disease (fig. S10, A and B, and table S11, A to C).

Using single-cell transcriptome profiling, we deconvoluted admixtures of cell types (e.g., pDCs, “intermediate” monocytes, cDC progenitors), revealed rare cell types (e.g., AS DCs), and elucidated complex relationships between cell types (e.g., spectrum of states for AS DCs)—thus addressing limitations in the existing classification that relies on a small number of markers (39). Nonetheless, some DC/monocyte subtypes were likely missed because they do not express MHC class II at rest, can only be defined by non-RNA molecules, are distinguished by low-abundance transcripts, or are only present during inflammation, disease, or within tissues. To build a comprehensive immune cell atlas, future studies will need to address these challenges as well as localize these cell types within lymphoid and nonlymphoid tissues.

Materials and methods

Study subjects

The study was performed in accordance with protocols approved by the institutional review board at Partners (Brigham and Women’s Hospital, Massachusetts General Hospital, Dana-Farber Cancer Institute; Boston, USA) and Broad Institute (USA), as well as the Newcastle upon Tyne Hospitals (UK) Research Ethics Committee. All patients provided written informed consent for the genetic research studies and molecular testing. Healthy donors were recruited from the Boston-based PhenoGenetic project, a resource of healthy subjects that are recontactable by genotype (57), and the Newcastle community. Individuals were excluded if they had a history of cancer, allergies, inflammatory disease, autoimmune disease, chronic metabolic disorders, or infectious disorders. All healthy donors were nonsmokers, had a normal BMI and normal blood pressure, and were between 25 and 40 years of age.

Cell isolation, flow cytometry staining, cell sorting, and analysis

For profiling of healthy cells, PBMCs were isolated from fresh blood within 2 hours of collection,

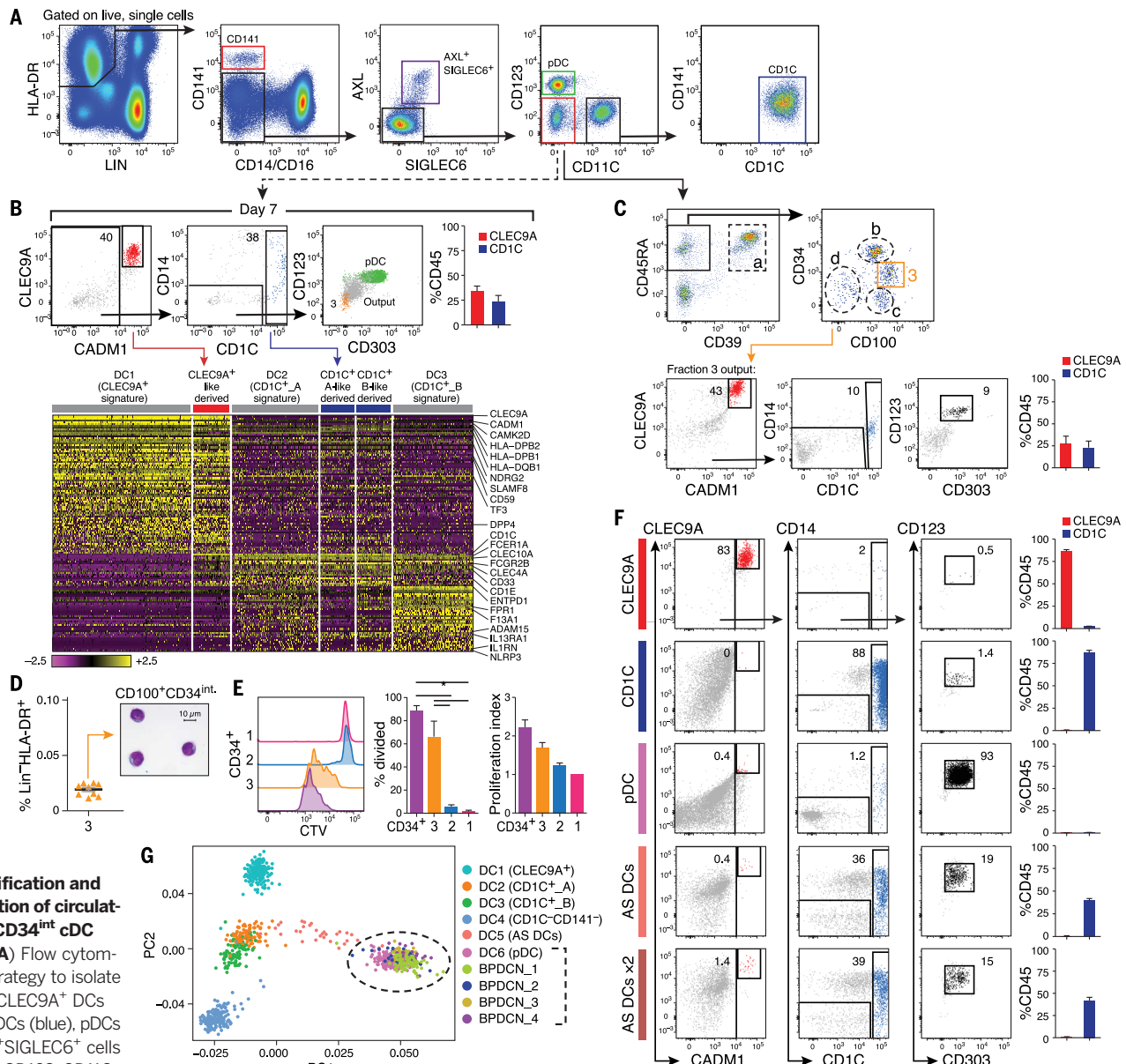


Fig. 6. Identification and characterization of circulating CD100^{hi}CD34^{int} cDC progenitor. (A) Flow cytometry gating strategy to isolate DC subsets: CLEC9A⁺ DCs (red), CD1C⁺ DCs (blue), pDCs (green), AXL⁺SIGLEC6⁺ cells (purple), and CD123⁻CD11C⁻

cells (red) for differentiation assays. Data shown are a representative analysis of at least 10 healthy individuals. (B) Differentiation assay readout (flow cytometry for CLEC9A⁺ DCs, CD1C⁺ DCs, and pDCs; scRNA-seq profiling of CD45⁺ cells) after 7 days of coculturing LIN(CD3, CD19, CD20, CD161)⁻HLA-DR⁺CD14⁻CD16⁻AXL⁺SIGLEC6⁺CD123⁻CD11C⁻ cells on MS5 stromal cell line supplemented with GM-CSF, SCF, and FLT3L. Top: Representative overlay dot plots. Overlay of pDC (green) and output cells (gray) for CD123 and CD303 expression is shown at far right (in green). Population 3 (in beige) represents CD100^{hi}CD34^{int} at day 0. Top right: Composite bar graphs for CLEC9A⁺ and CD1C⁺ DCs differentiated from culture by flow cytometry analysis ($n = 4$, mean \pm SEM). Heat map in bottom panel reports scaled expression (log TPM values) signature from culture output by scRNA-seq ($n = 132$) confirming differentiated CLEC9A⁺ (red) and CD1C⁺ (blue) DC transcriptional identities. Original transcriptional signatures from DC1 (CD141⁺/CLEC9A⁺ DC), DC2 (CD1C_A subset), and DC3 (CD1C_B subset) clusters are used as reference set. (C) Top: Flow cytometry gating strategy used to identify the CD100^{hi}CD34^{int} subset. All cell fractions in dashed gate were tested for differentiation potential (see fig. S6, A to F). Bottom: Output from CD100^{hi}CD34^{int} fraction (population 3, beige gate). (D) Frequency of CD100^{hi}CD34^{int} subset as of

LIN(CD3, CD19, CD20, CD161)⁻HLA-DR⁺ PBMCs ($n = 9$ healthy donors). Morphology of CD100^{hi}CD34^{int} cell by Giemsa-Wright stain. Scale bar, 10 μ m. (E) Proliferative capacity of peripheral blood Cell Trace Violet (CTV)-labeled CD34⁺ HSCs (purple), CD100^{hi}CD34^{int} (beige), AXL⁺SIGLEC6⁺CD123⁺CD11C^{-lo} (pink), and AXL⁺SIGLEC6⁺CD123^{lo}CD11C⁺ (blue), as measured by CTV dilution after 5 days in culture on MS5 stromal cell line supplemented with GM-CSF, SCF, and FLT3LG. Left: Representative overlay histogram. Right: Composite bar graphs illustrating percentage of proliferated cells and number of proliferations undergone from three donors shown (* $P < 0.05$, paired *t* test). (F) Output from differentiation assays seeded with CLEC9A⁺ DCs, CD1C⁺ DCs, pDCs, and AXL⁺SIGLEC6⁺ cells isolated using gating strategy in (A). AXL⁺SIGLEC6^{x2} = double FLT3L concentration. Also shown in (C) and (F) are representative culture outputs on day 7 and composite bar graphs (mean \pm SEM; $n = 6$ donors). (G) PCA analysis incorporating monocytes ($n = 339$), DCs ($n = 742$), and four BPDCN patient samples ($n = 174$) using the R software package Seurat. PC1 versus PC2 demonstrates the close transcriptional proximity between the four BPDCN samples and pDCs (dashed black circle); black bracket indicates overlapping cells. PC1 and PC2 variance is 3.8%. Each dot represents an individual cell; colored legend for each subset is shown at the right.

using Ficoll-Paque density gradient centrifugation as described (58). Single-cell suspensions were stained per manufacturer recommendations with different panels of antibodies (table S12) designed to enrich for certain population for single-cell sorting and single-cell RNA sequencing (scRNA-seq) (6). Flow cytometry and FACS sorting of PBMCs was performed on a BD Fortessa or BD FACS Fusion instrument, and data analyzed using FlowJov10.1. Single cells were sorted into 96-well full-skirted Eppendorf plates chilled to 4°C, prepared with lysis buffer consisting of 10 µl of TCL buffer (Qiagen) supplemented with 1% β-mercaptoethanol. Single-cell lysates were sealed, vortexed, spun down at 300 g at 4°C for 1 min, immediately placed on dry ice, and transferred for storage at -80°C. Tonsil was mechanically disrupted to obtain single-cell suspension.

Single-cell RNA sequencing

Smart-Seq2 protocol was performed on single sorted cells as described (7, 8), with some modifications (6). For DCs, a total of 8 × 96-well plates (768 single DCs) were initially profiled from the same blood draw and sort from the index volunteer and subsequent validation performed on an additional 10 healthy individuals. For monocytes, a total of four plates were profiled (372 single monocytes and 12 population samples). An additional 975 single cells were profiled to further characterize the CD1C⁺ DC subsets (*n* = 125), AXL⁺SIGLEC6⁺ cells (*n* = 372), CD11C⁻CD123⁺ compartment at day 0 (*n* = 164), differentiation assay outputs (*n* = 218), CD100^{hi}CD34^{int} cells (*n* = 96), and BPDCN patient samples (*n* = 269). Note that some of these single cells were excluded from the analysis after applying QC filters and analytically confirming cell type (6).

Single-cell RNA sequencing analyses

Raw sequencing data were processed as described (59) (see tables S13 to S16 for cell identities that accompany raw data and gene expression matrices). Briefly, short sequencing reads were aligned to the UCSC hg19 transcriptome. These alignments were used to estimate transcriptomic alignment rates and were also used as input in RSEM v 1.2.1 to quantify gene expression levels (transcripts per million; TPM) for all UCSC hg19 genes in all samples. We filtered out low-quality cells from our data set based on a threshold for the number of genes detected (a minimum of 3000 unique genes per cell for cells sequenced at HiSeq depth, and 2000 unique genes per cell for cells sequenced at MiSeq depth). All genes that were not detected in at least 0.5% of all our single cells were discarded, leaving 21,581 genes for all further analyses. Data were log-transformed [$\log(\text{TPM} + 1)$] for all downstream analyses, most of which were performed using the R software package Seurat (<https://github.com/satijalab/seurat>; <http://satijalab.org/seurat/>). See (6) for further details, including R script used to generate clusters.

DC differentiation assay on MS5 stromal cells

DC differentiation assay was performed as described (23–25) with minor adaptation. Briefly, 1 ×

10^4 purified progenitors, DCs, and monocyte subsets were cultured in 96-well flat-bottom plates layered with 4×10^4 murine MS5 stromal cells (DSMZ, Germany) in the presence of human FLT3 ligand (FL; 100 ng/ml; Miltenyi Biotech), recombinant human SCF (20 ng/ml; R&D Systems), and recombinant human granulocyte-macrophage colony-stimulating factor (GM-CSF) (10 ng/ml; Peprotech). MS5 stromal cells were seeded 24 hours prior to coculture. Growth factors were replenished on day 3 of culture. Cells were in culture for up to 7 days prior to harvesting by physical dissociation on ice. Cells were then stained on ice either for flow cytometry analysis (see output panel in table S12) or single-cell index sorting of CD45⁺ cells for scRNA-seq of culture output analysis.

Cytokine production measurements

Purified subsets were cultured at 5×10^3 cells per well in 96-well round-bottom plates in the presence of LPS (100 ng/ml; Invivogen) and ODN2395 (1 µM; Invivogen) or ODN5328 (ODN2395 control, 1 µM; Invivogen), or in the presence of LPS, poly(I:C) (25 µg/ml; Invivogen), and R848 (2.5 µg/ml; Enzo Life Sciences). Culture supernatants were harvested after 24 hours and analyzed using a multiplexed cytokine assay (ProcartaPlex, eBioscience), or by leveraging the 92 inflammatory-related protein biomarker panel and four controls provided by Olink Proteomics (Uppsala, Sweden) (6).

Assessing T cell stimulatory potential

DC, monocyte, and progenitor subsets were purified from peripheral blood of healthy donors by FACS sorting (BD FACS Fusion; see table S12 for sorting panels and antibodies). For T cell stimulatory potential, purified DCs, monocytes, AXL⁺SIGLEC6⁺ subsets, and progenitor subset were cultured at cell density of 5×10^4 per well. All purified cell subsets were matured with LPS (100 ng/ml, Sigma) and R848 (2.5 µg/ml, Invivogen), or with just LPS (100 ng/ml), for 24 hours prior to coculture with 5×10^5 CFSE-labeled allogeneic unfractionated CD3⁺ T cells at a 1:10 DC:T cell ratio. T cell proliferation was assessed by measuring CFSE dilution on day 5 of culture.

Cytospin and immunostaining

Cytospin of FACS-purified cells was prepared as described (60) using Shandon Cytospin 4 (Thermo Scientific). Giemsa-Wright staining was performed using Advia S60 (Siemens) and imaged using Axioimager.Z2 microscope with Axiovision software v4.8 (Carl Zeiss, Germany). Human tonsil paraffin sections were immunostained with the antibodies anti-AXL (MM0098-2N33, Abcam), CD123 (BR4MS, Leica Biosystems) and CD3 (LN10, Leica Biosystems) using a Ventana Benchmark XT instrument.

Monitoring cell proliferation

PBMCs were labeled with Cell Trace Violet (CTV, Life Technologies) according to manufacturer's protocol. CTV-labeled FACS-purified progenitors and DC subsets were cultured on murine MS5 stromal cells as described above and analyzed on day 5 to assess proliferation measured by CTV dilution.

REFERENCES AND NOTES

- M. Haniffa, V. Bigley, M. Collin, Human mononuclear phagocyte system reunited. *Semin. Cell Dev. Biol.* **41**, 59–69 (2015). doi: [10.1016/j.semcd.2015.05.004](https://doi.org/10.1016/j.semcd.2015.05.004); pmid: [25986054](https://pubmed.ncbi.nlm.nih.gov/25986054/)
- A. Mildner, S. Jung, Development and function of dendritic cell subsets. *Immunity* **40**, 642–656 (2014). doi: [10.1016/j.immuni.2014.04.016](https://doi.org/10.1016/j.immuni.2014.04.016); pmid: [25553392](https://pubmed.ncbi.nlm.nih.gov/25553392/)
- B. U. Schraml, C. Reis e Sousa, Defining dendritic cells. *Curr. Opin. Immunol.* **32**, 13–20 (2015). doi: [10.1016/j.co.2014.11.001](https://doi.org/10.1016/j.co.2014.11.001); pmid: [25553392](https://pubmed.ncbi.nlm.nih.gov/25553392/)
- C. Trapnell, Defining cell types and states with single-cell genomics. *Genome Res.* **25**, 1491–1498 (2015). doi: [10.1101/gr.190595.115](https://doi.org/10.1101/gr.190595.115); pmid: [26430159](https://pubmed.ncbi.nlm.nih.gov/26430159/)
- D. Grün, A. van Oudenaarden, Design and analysis of single-cell sequencing experiments. *Cell* **163**, 799–810 (2015). doi: [10.1016/j.cell.2015.10.039](https://doi.org/10.1016/j.cell.2015.10.039); pmid: [26544934](https://pubmed.ncbi.nlm.nih.gov/26544934/)
- See supplementary materials.
- S. Picelli et al., Smart-seq2 for sensitive full-length transcriptome profiling in single cells. *Nat. Methods* **10**, 1096–1098 (2013). doi: [10.1038/nmeth.2639](https://doi.org/10.1038/nmeth.2639); pmid: [24056875](https://pubmed.ncbi.nlm.nih.gov/24056875/)
- J. J. Trombetta et al., *Curr. Protoc. Mol. Biol.* **107**, 4.22.1–4.22.17 (2014).
- E. Z. Macosko et al., Highly parallel genome-wide expression profiling of individual cells using nanoliter droplets. *Cell* **161**, 1202–1214 (2015). doi: [10.1016/j.cell.2015.05.002](https://doi.org/10.1016/j.cell.2015.05.002); pmid: [26000488](https://pubmed.ncbi.nlm.nih.gov/26000488/)
- L. van der Maaten, G. Hinton, Visualizing data using t-SNE. *J. Machine Learn. Res.* **9**, 2579–2605 (2008). www.jmlr.org/papers/volume9/vandermaaten08a/vandermaaten08a.pdf doi: [10.1162/jmlr.2008.9.9.2579](https://doi.org/10.1162/jmlr.2008.9.9.2579); pmid: [26095251](https://pubmed.ncbi.nlm.nih.gov/26095251/)
- J. H. Levine et al., Data-driven phenotypic dissection of AML reveals progenitor-like cells that correlate with prognosis. *Cell* **162**, 184–197 (2015). doi: [10.1016/j.cell.2015.05.047](https://doi.org/10.1016/j.cell.2015.05.047); pmid: [26095251](https://pubmed.ncbi.nlm.nih.gov/26095251/)
- H. Liu, J. Liu, M. Toups, T. Soos, C. Arendt, Gene signature-based mapping of immunological systems and diseases. *BMC Bioinformatics* **17**, 171 (2016). doi: [10.1186/s12859-016-1012-y](https://doi.org/10.1186/s12859-016-1012-y); pmid: [27089880](https://pubmed.ncbi.nlm.nih.gov/27089880/)
- V. Pascual, D. Chaussabel, J. Banchereau, A genomic approach to human autoimmune diseases. *Annu. Rev. Immunol.* **28**, 535–571 (2010). doi: [10.1146/annurev-immunol-030409-101221](https://doi.org/10.1146/annurev-immunol-030409-101221); pmid: [20192809](https://pubmed.ncbi.nlm.nih.gov/20192809/)
- B. Mesko, S. Poliska, L. Nagy, Gene expression profiles in peripheral blood for the diagnosis of autoimmune diseases. *Trends Mol. Med.* **17**, 223–233 (2011). doi: [10.1016/j.molmed.2010.12.004](https://doi.org/10.1016/j.molmed.2010.12.004); pmid: [21388884](https://pubmed.ncbi.nlm.nih.gov/21388884/)
- R. S. Welner et al., Interferon-producing killer dendritic cells (IKDCs) arise via a unique differentiation pathway from primitive c-kit/HCD62L⁺ lymphoid progenitors. *Blood* **109**, 4825–4931 (2007). doi: [10.1182/blood-2006-08-043810](https://doi.org/10.1182/blood-2006-08-043810); pmid: [17317852](https://pubmed.ncbi.nlm.nih.gov/17317852/)
- J. Taube et al., A novel dendrite cell subset involved in tumor immunosurveillance. *Nat. Med.* **12**, 214–219 (2006). doi: [10.1038/nm1356](https://doi.org/10.1038/nm1356); pmid: [16444265](https://pubmed.ncbi.nlm.nih.gov/16444265/)
- C. W. Chan et al., Interferon-producing killer dendritic cells provide a link between innate and adaptive immunity. *Nat. Med.* **12**, 207–213 (2006). doi: [10.1038/nm1352](https://doi.org/10.1038/nm1352); pmid: [16444266](https://pubmed.ncbi.nlm.nih.gov/16444266/)
- M. Siewecki, M. Colonna, The multifaceted biology of plasmacytoid dendritic cells. *Nat. Rev. Immunol.* **15**, 471–485 (2015). doi: [10.1038/nri3865](https://doi.org/10.1038/nri3865); pmid: [26160613](https://pubmed.ncbi.nlm.nih.gov/26160613/)
- M. Cheng et al., Characterization of species-specific genes regulated by E2-2 in human plasmacytoid dendritic cells. *Sci. Rep.* **5**, 10752 (2015). doi: [10.1038/srep10752](https://doi.org/10.1038/srep10752); pmid: [26182859](https://pubmed.ncbi.nlm.nih.gov/26182859/)
- T. Matsui et al., CD2 distinguishes two subsets of human plasmacytoid dendritic cells with distinct phenotype and functions. *J. Immunol.* **182**, 6815–6823 (2009). doi: [10.4049/jimmunol.0802008](https://doi.org/10.4049/jimmunol.0802008); pmid: [19454677](https://pubmed.ncbi.nlm.nih.gov/19454677/)
- G. Grouard et al., The enigmatic plasmacytoid T cells develop into dendrite cells with interleukin (IL)-3 and CD40-ligand. *J. Exp. Med.* **185**, 1101–1111 (1997). doi: [10.1084/jem.185.6.1101](https://doi.org/10.1084/jem.185.6.1101); pmid: [9091583](https://pubmed.ncbi.nlm.nih.gov/9091583/)
- J. C. Miller et al., Deciphering the transcriptional network of the dendrite cell lineage. *Nat. Immunol.* **13**, 888–899 (2012). doi: [10.1038/ni.2370](https://doi.org/10.1038/ni.2370); pmid: [22797772](https://pubmed.ncbi.nlm.nih.gov/22797772/)
- A. T. Satpathy, X. Wu, J. C. Albring, K. M. Murphy, Re(de)fining the dendrite cell lineage. *Nat. Immunol.* **13**, 1145–1154 (2012). doi: [10.1038/ni.2467](https://doi.org/10.1038/ni.2467); pmid: [23160217](https://pubmed.ncbi.nlm.nih.gov/23160217/)
- G. Breton et al., Circulating precursors of human CD1c⁺ and CD141⁺ dendrite cells. *J. Exp. Med.* **212**, 401–413 (2015). doi: [10.1084/jem.20141441](https://doi.org/10.1084/jem.20141441); pmid: [25687281](https://pubmed.ncbi.nlm.nih.gov/25687281/)
- J. Lee et al., Restricted dendrite cell and monocyte progenitors in human cord blood and bone marrow. *J. Exp.*

- Med.* **212**, 385–399 (2015). doi: [10.1084/jem.20141442](https://doi.org/10.1084/jem.20141442); pmid: [25687283](https://pubmed.ncbi.nlm.nih.gov/25687283/)
26. G. Breton, J. Lee, K. Liu, M. C. Nussenzweig, Defining human dendritic cell progenitors by multiparametric flow cytometry. *Nat. Protoc.* **10**, 1407–1422 (2015). doi: [10.1038/nprot.2015.092](https://doi.org/10.1038/nprot.2015.092); pmid: [26292072](https://pubmed.ncbi.nlm.nih.gov/26292072/)
27. F. Notta *et al.*, Distinct routes of lineage development reshape the human blood hierarchy across ontogeny. *Science* **351**, aab2116 (2016). doi: [10.1126/science.aab2116](https://doi.org/10.1126/science.aab2116); pmid: [26541609](https://pubmed.ncbi.nlm.nih.gov/26541609/)
28. S. Doulatov, F. Notta, E. Laurenti, J. E. Dick, Hematopoiesis: A human perspective. *Cell Stem Cell* **10**, 120–136 (2012). doi: [10.1016/j.stem.2012.01.006](https://doi.org/10.1016/j.stem.2012.01.006); pmid: [22305562](https://pubmed.ncbi.nlm.nih.gov/22305562/)
29. K. Hildner *et al.*, Batf3 deficiency reveals a critical role for CD8α⁺ dendritic cells in cytotoxic T cell immunity. *Science* **322**, 1097–1100 (2008). doi: [10.1126/science.1164206](https://doi.org/10.1126/science.1164206); pmid: [19008445](https://pubmed.ncbi.nlm.nih.gov/19008445/)
30. L. F. Poulin *et al.*, Characterization of human DNLR-1⁺ BDCA3⁺ leukocytes as putative equivalents of mouse CD8α⁺ dendritic cells. *J. Exp. Med.* **207**, 1261–1271 (2010). doi: [10.1084/jem.20092618](https://doi.org/10.1084/jem.20092618); pmid: [20479117](https://pubmed.ncbi.nlm.nih.gov/20479117/)
31. K. Crozat *et al.*, The XC chemokine receptor 1 is a conserved selective marker of mammalian cells homologous to mouse CD8α⁺ dendritic cells. *J. Exp. Med.* **207**, 1283–1292 (2010). doi: [10.1084/jem.20100223](https://doi.org/10.1084/jem.20100223); pmid: [20479118](https://pubmed.ncbi.nlm.nih.gov/20479118/)
32. S. L. Jongbloed *et al.*, Human CD141⁺ (BDCA-3)⁺ dendritic cells (DCs) represent a unique myeloid DC subset that cross-presents necrotic cell antigens. *J. Exp. Med.* **207**, 1247–1260 (2010). doi: [10.1084/jem.20092140](https://doi.org/10.1084/jem.20092140); pmid: [20479116](https://pubmed.ncbi.nlm.nih.gov/20479116/)
33. M. Haniffa *et al.*, Human tissues contain CD141hi cross-presenting dendritic cells with functional homology to mouse CD103⁺ nonlymphoid dendritic cells. *Immunity* **37**, 60–73 (2012). doi: [10.1016/j.immuni.2012.04.012](https://doi.org/10.1016/j.immuni.2012.04.012); pmid: [22795876](https://pubmed.ncbi.nlm.nih.gov/22795876/)
34. W. Riaz, L. Zhang, P. Horna, L. Sokol, *Cancer Contr.* **21**, 279–289 (2014).
35. F. Garnache-Ottou, J. Feuillard, P. Saas, Plasmacytoid dendritic cell leukaemia/lymphoma: Towards a well defined entity? *Br. J. Haematol.* **136**, 539–548 (2007). doi: [10.1111/j.1365-2141.2006.06458.x](https://doi.org/10.1111/j.1365-2141.2006.06458.x); pmid: [17367408](https://pubmed.ncbi.nlm.nih.gov/17367408/)
36. M. R. Sapienza *et al.*, Molecular profiling of blastic plasmacytoid dendritic cell neoplasm reveals a unique pattern and suggests selective sensitivity to NF-κB pathway inhibition. *Leukemia* **28**, 1606–1616 (2014). doi: [10.1038/leu.2014.64](https://doi.org/10.1038/leu.2014.64); pmid: [24504027](https://pubmed.ncbi.nlm.nih.gov/24504027/)
37. Y. Osaki *et al.*, Characterization of CD56⁺ dendritic-like cells: A normal counterpart of blastic plasmacytoid dendritic cell neoplasm? *PLOS ONE* **8**, e81722 (2013). doi: [10.1371/journal.pone.0081722](https://doi.org/10.1371/journal.pone.0081722); pmid: [24312342](https://pubmed.ncbi.nlm.nih.gov/24312342/)
38. H. Yu *et al.*, Human BDCA2⁺CD123⁺CD56⁺ dendritic cells (DCs) related to blastic plasmacytoid dendritic cell neoplasm represent a unique myeloid DC subset. *Protein Cell* **6**, 297–306 (2015). doi: [10.1007/s13238-015-0140-x](https://doi.org/10.1007/s13238-015-0140-x); pmid: [25779340](https://pubmed.ncbi.nlm.nih.gov/25779340/)
39. M. Guilliams *et al.*, Dendritic cells, monocytes and macrophages: A unified nomenclature based on ontogeny. *Nat. Rev. Immunol.* **14**, 571–578 (2014). doi: [10.1038/nri3712](https://doi.org/10.1038/nri3712); pmid: [25033907](https://pubmed.ncbi.nlm.nih.gov/25033907/)
40. K. L. Lewis *et al.*, Notch2 receptor signaling controls functional differentiation of dendritic cells in the spleen and intestine. *Immunity* **35**, 780–791 (2011). doi: [10.1016/j.immuni.2011.08.013](https://doi.org/10.1016/j.immuni.2011.08.013); pmid: [22018469](https://pubmed.ncbi.nlm.nih.gov/22018469/)
41. A. T. Satpathy *et al.*, Notch2-dependent classical dendritic cells orchestrate intestinal immunity to attaching-and-effacing bacterial pathogens. *Nat. Immunol.* **14**, 937–948 (2013). doi: [10.1038/ni.2679](https://doi.org/10.1038/ni.2679); pmid: [23913046](https://pubmed.ncbi.nlm.nih.gov/23913046/)
42. A. Schlitzer *et al.*, IRF4 transcription factor-dependent CD11b⁺ dendritic cells in human and mouse control mucosal IL-17 cytokine responses. *Immunity* **38**, 970–983 (2013). doi: [10.1016/j.immuni.2013.04.011](https://doi.org/10.1016/j.immuni.2013.04.011); pmid: [23706669](https://pubmed.ncbi.nlm.nih.gov/23706669/)
43. E. K. Persson *et al.*, IRF4 transcription-factor-dependent CD103⁺CD11b⁺ dendritic cells drive mucosal T helper 17 cell differentiation. *Immunity* **38**, 958–969 (2013). doi: [10.1016/j.immuni.2013.03.009](https://doi.org/10.1016/j.immuni.2013.03.009); pmid: [23664832](https://pubmed.ncbi.nlm.nih.gov/23664832/)
44. M. S. Macauley, P. R. Crocker, J. C. Paulson, Siglec-mediated regulation of immune cell function in disease. *Nat. Rev. Immunol.* **14**, 653–666 (2014). doi: [10.1038/nri3737](https://doi.org/10.1038/nri3737); pmid: [25234143](https://pubmed.ncbi.nlm.nih.gov/25234143/)
45. C. V. Rothlin, E. A. Carrera-Silva, L. Bosurgi, S. Ghosh, TAM receptor signaling in immune homeostasis. *Annu. Rev. Immunol.* **33**, 355–391 (2015). doi: [10.1146/annurev-immunol-032414-112103](https://doi.org/10.1146/annurev-immunol-032414-112103); pmid: [25594431](https://pubmed.ncbi.nlm.nih.gov/25594431/)
46. T. J. Nowakowski *et al.*, Expression analysis highlights AXL as a candidate Zika virus entry receptor in neural stem cells. *Cell Stem Cell* **18**, 591–596 (2016). doi: [10.1016/j.stem.2016.03.012](https://doi.org/10.1016/j.stem.2016.03.012); pmid: [27038591](https://pubmed.ncbi.nlm.nih.gov/27038591/)
47. L. Bar-On *et al.*, CX3CR1⁺ CD8α⁺ dendritic cells are a steady-state population related to plasmacytoid dendritic cells. *Proc. Natl. Acad. Sci. U.S.A.* **107**, 14745–14750 (2010). doi: [10.1073/pnas.1001562107](https://doi.org/10.1073/pnas.1001562107); pmid: [20679228](https://pubmed.ncbi.nlm.nih.gov/20679228/)
48. C. M. Lau *et al.*, Leukemia-associated activating mutation of Flt3 expands dendrite cells and alters T cell responses. *J. Exp. Med.* **213**, 415–431 (2016). doi: [10.1084/jem.20150642](https://doi.org/10.1084/jem.20150642); pmid: [26903243](https://pubmed.ncbi.nlm.nih.gov/26903243/)
49. T. R. Wilhelm *et al.*, Siglec-1-positive plasmacytoid dendritic cells (pDCs) in human peripheral blood: A semi-mature and myeloid-like subset imbalanced during protective and autoimmune responses. *Clin. Immunol.* **163**, 42–51 (2016). doi: [10.1016/j.clim.2015.12.001](https://doi.org/10.1016/j.clim.2015.12.001); pmid: [26674280](https://pubmed.ncbi.nlm.nih.gov/26674280/)
50. N. Schwab, A. L. Zozulya, B. C. Kieseier, K. V. Toyka, H. Wiendl, An imbalance of two functionally and phenotypically different subsets of plasmacytoid dendritic cells characterizes the dysfunctional immune regulation in multiple sclerosis. *J. Immunol.* **184**, 5368–5374 (2010). doi: [10.4049/jimmunol.0903662](https://doi.org/10.4049/jimmunol.0903662); pmid: [20357264](https://pubmed.ncbi.nlm.nih.gov/20357264/)
51. Q. Du *et al.*, Preferential depletion of CD2^{low} plasmacytoid dendritic cells in HIV-infected subjects. *Cell. Mol. Immunol.* **8**, 441–444 (2011). doi: [10.1038/cmi.2011.9](https://doi.org/10.1038/cmi.2011.9); pmid: [21516119](https://pubmed.ncbi.nlm.nih.gov/21516119/)
52. C. Bryant *et al.*, A CD2 high-expressing stress-resistant human plasmacytoid dendritic-cell subset. *Immunol. Cell Biol.* **94**, 447–457 (2016). doi: [10.1038/icb.2015.116](https://doi.org/10.1038/icb.2015.116); pmid: [26791160](https://pubmed.ncbi.nlm.nih.gov/26791160/)
53. M. Celli *et al.*, Plasmacytoid monocytes migrate to inflamed lymph nodes and produce large amounts of type I interferon. *Nat. Med.* **5**, 919–923 (1999). doi: [10.1038/11360](https://doi.org/10.1038/11360); pmid: [10426316](https://pubmed.ncbi.nlm.nih.gov/10426316/)
54. J. De Vries, C. Figdor, Immunotherapy: Cancer vaccine triggers antiviral-type defences. *Nature* **534**, 329–331 (2016). doi: [10.1038/nature18443](https://doi.org/10.1038/nature18443); pmid: [27281206](https://pubmed.ncbi.nlm.nih.gov/27281206/)
55. J. Tel *et al.*, Human plasmacytoid dendrite cells are equipped with antigen-presenting and tumoricidal capacities. *Blood* **120**, 3936–3944 (2012). doi: [10.1182/blood-2012-06-435941](https://doi.org/10.1182/blood-2012-06-435941); pmid: [22966165](https://pubmed.ncbi.nlm.nih.gov/22966165/)
56. J. Tel *et al.*, Natural human plasmacytoid dendrite cells induce antigen-specific T-cell responses in melanoma patients. *Cancer Res.* **73**, 1063–1075 (2013). doi: [10.1158/0008-5472-CAN-12-2583](https://doi.org/10.1158/0008-5472-CAN-12-2583); pmid: [23345163](https://pubmed.ncbi.nlm.nih.gov/23345163/)
57. Z. Xia *et al.*, A 17q12 allele is associated with altered NK cell subsets and function. *J. Immunol.* **188**, 3315–3322 (2012). doi: [10.4049/jimmunol.1102775](https://doi.org/10.4049/jimmunol.1102775); pmid: [22345646](https://pubmed.ncbi.nlm.nih.gov/22345646/)
58. M. N. Lee *et al.*, Common genetic variants modulate pathogen-sensing responses in human dendrite cells. *Science* **343**, 1246980 (2014). doi: [10.1126/science.1246980](https://doi.org/10.1126/science.1246980); pmid: [24604203](https://pubmed.ncbi.nlm.nih.gov/24604203/)
59. A. K. Shalek *et al.*, Single-cell RNA-seq reveals dynamic paracrine control of cellular variation. *Nature* **510**, 363–369 (2014). pmid: [24919153](https://pubmed.ncbi.nlm.nih.gov/24919153/)
60. M. Haniffa *et al.*, Differential rates of replacement of human dermal dendrite cells and macrophages during hematopoietic stem cell transplantation. *J. Exp. Med.* **206**, 371–385 (2009). doi: [10.1084/jem.20081633](https://doi.org/10.1084/jem.20081633); pmid: [19171766](https://pubmed.ncbi.nlm.nih.gov/19171766/)

ACKNOWLEDGMENTS

We thank the subjects in the PhenoGenetic Project for donating the blood used in our study; E. Segura, S. Amigorena, C. Benoit, and D. Puyraimond-Zemmour for advice on the sorting strategy; M. Waring and the Ragon Institute Imaging Core-Flow Cytometry Facility [which is supported in part by the Harvard University Center for AIDS Research (CFAR), an NIH-funded program (5 P30 AI060354-10)]; T. Booth and Newcastle University Biomechanics Unit for assistance with microscopy; L. Gaffney for illustrations; and A. Long from MRC/EPSRC Molecular Pathology Node, J. Scott, K. Best, C. Jones, D. Lieb, C. Ford, D. Gennert, J. Trombetta, and A. Schnell for help and advice. Supported by National Human Genome Research Institute Centers of Excellence in Genomics Science grant P50 HG006193 (N.H. and A.R.), Manton Foundation (A.R. and N.H.), Howard Hughes Medical Institute (A.R.), NIH BRAIN grant (A.R.), Klarman Family Foundation (A.R. and N.H.), Banting Postdoctoral Fellowship (A.C.V.), NIH Director's New Innovator Award Program DP2-HG-009623 (R.S.), American Society of Hematology Scholar grant (A.A.L.), ISAC SRL-EL program (A.J.F.), and Wellcome Trust grants WT088555 and WT107931/Z/15/Z (M.H., A.C.V., R.S., A.R., N.H.), the Broad Institute, and Massachusetts General Hospital have filed a U.S. provisional patent application (62/376,007) that relates to products and methods useful for modulating and evaluating immune responses. A.R. is a scientific advisory board member for ThermoFisher Scientific and Syros Pharmaceuticals and a consultant for Driver Group. Processed scRNA-seq data are available through the Gene Expression Omnibus, accession number GSE94820, and through the Broad Institute Single Cell Portal at https://portals.broadinstitute.org/single_cell/study/atlas-of-human-blood-dendrite-cells-and-monocytes. Raw RNA sequencing data are available through Database of Genotypes and Phenotypes (dbGaP), accession number phs001294.v1.p1.

SUPPLEMENTARY MATERIALS

www.science.org/content/356/6335/eaah4573/suppl/DC1
Materials and Methods
Figs. S1 to S11
Tables S1 to S16
References (61–77)

29 June 2016; accepted 7 March 2017
10.1126/science.aaah4573

Single-cell RNA-seq reveals new types of human blood dendritic cells, monocytes, and progenitors

Alexandra-Chloé Villani, Rahul Satija, Gary Reynolds, Siranush Sarkizova, Karthik Shekhar, James Fletcher, Morgane Griesbeck, Andrew Butler, Shiwei Zheng, Suzan Lazo, Laura Jardine, David Dixon, Emily Stephenson, Emil Nilsson, Ida Grundberg, David McDonald, Andrew Filby, Weibo Li, Philip L. De Jager, Orit Rozenblatt-Rosen, Andrew A. Lane, Muzlifah Haniffa, Aviv Regev and Nir Hacohen

Science 356 (6335), eaah4573.
DOI: 10.1126/science.aah4573

What's in a drop of blood?

Blood contains many types of cells, including many immune system components. Immune cells used to be characterized by marker-based assays, but now classification relies on the genes that cells express. Villani *et al.* used deep sequencing at the single-cell level and unbiased clustering to define six dendritic cell and four monocyte populations. This refined analysis has identified, among others, a previously unknown dendritic cell population that potently activates T cells. Further cell culture revealed possible differentiation progenitors within the different cell populations.

Science, this issue p. eaah4573

ARTICLE TOOLS

<http://science.scienmag.org/content/356/6335/eaah4573>

SUPPLEMENTARY MATERIALS

<http://science.scienmag.org/content/suppl/2017/04/19/356.6335.eaah4573.DC1>

REFERENCES

This article cites 74 articles, 20 of which you can access for free
<http://science.scienmag.org/content/356/6335/eaah4573#BIBL>

PERMISSIONS

<http://www.scienmag.org/help/reprints-and-permissions>

Use of this article is subject to the [Terms of Service](#)

Science (print ISSN 0036-8075; online ISSN 1095-9203) is published by the American Association for the Advancement of Science, 1200 New York Avenue NW, Washington, DC 20005. The title *Science* is a registered trademark of AAAS.

Copyright © 2017, American Association for the Advancement of Science